Electrical Resistivity Tomography Protocol for Landfill Monitoring

by

Juan Chavez Olalla

in partial fulfillment of the requirements for the degree of

Master of Science in Civil Engineering

at the Delft University of Technology, to be defended publicly on Friday July 28, 2017 at 3:00 PM.

Supervisor: Prof. dr. ir. T.J. Heimovaara

Thesis committee: Dr. ir. D. S. Draganov, TU Delft

Dr. ir. D. J. M. Ngan-Tillard TU Delft

An electronic version of this thesis is available at http://repository.tudelft.nl/.



Abstract

Aftercare of sanitary landfills represents a burden for future generations, for emission potential of leachate and gases remains for hundred of years. Treatment methods have to be developed in order to accelerate waste degradation and reduce emission potential preferably within the time-span of one generation. Aeration seems a promising treatment method but as yet has to be proven effective as a methodology to enhance waste degradation at full scale. Water content plays a crucial role in evaluating aeration, but the highly heterogeneous nature of a landfill body poses a big uncertainty in quantifying it and therefore also quantifying the effectiveness of aeration in reducing emission potential. To improve understanding of water within a waste body, Electrical Resistivity Tomography ERT is to be used to indirectly measure water content by obtaining electric resistivity information. However, full scale landfills have large areas and therefore a protocol needs to be developed for generating an optimum survey strategy, so that high resolution information is obtained while covering a large area. This thesis presents such a protocol consisting of four parts. First, optimum spread and spacing are defined by building a Pareto front with resolution and covered area as objective criteria. Second, array is designed in the previously defined grid, with standard and non-standard four-electrode configurations, by using a goodness function applied to multiple channel acquisition systems. Third, array design is tested with synthetic models showing that smooth resistivity models are well captured by data inversion, but array design performs poorly in a sharp resistivity model. Finally, practical aspects namely injection time, polarization effects and unstable configurations which are usually overlooked, are shown to have significant influence in data quality. This protocol is intended as a systematic approach to generate an optimum ERT survey strategy which could be extended to other geophysical methods.

Contents

1		roduction	1
		Justification	
	1.2	Research question	2
2		thodology	3
		General approach	
	2.2	Part I: Spread and spacing	
		2.2.1 Model resolution	
	0.0	2.2.2 Covered area	
	2.3	Part II: Array design	
	0.4	2.3.1 Goodness function	
	2.4	Part III: Array performance in synthetic data	
		2.4.1 Water flow model	
	۰	2.4.2 Checker board model	
	2.5	Part IV: Practical aspects for data acquisition	
		2.5.1 Injection time	
		2.5.2 Polarization effects	
		2.5.3 Geometrically unstable configurations	9
3	Res		11
3		Bults Description of the case study	
3	3.1		11
3	3.1 3.2	Description of the case study	11 12
3	3.1 3.2 3.3	Description of the case study	11 12 15
3	3.1 3.2 3.3	Description of the case study	11 12 15 16
3	3.1 3.2 3.3 3.4	Description of the case study. Part I: Spread and spacing Part II: Array design Part III: Array performance in synthetic data 3.4.1 Performance optimized design in water flow model 3.4.2 Performance optimized design in checkerboard	11 12 15 16 16 18
3	3.1 3.2 3.3 3.4	Description of the case study	11 12 15 16 16 18
3	3.1 3.2 3.3 3.4	Description of the case study. Part I: Spread and spacing Part II: Array design Part III: Array performance in synthetic data 3.4.1 Performance optimized design in water flow model 3.4.2 Performance optimized design in checkerboard	11 12 15 16 16 18
	3.1 3.2 3.3 3.4 3.5	Description of the case study. Part I: Spread and spacing	11 12 15 16 16 18
	3.1 3.2 3.3 3.4 3.5	Description of the case study. Part I: Spread and spacing	11 12 15 16 16 18 18 18
	3.1 3.2 3.3 3.4 3.5 Disc 4.1	Description of the case study. Part I: Spread and spacing Part II: Array design Part III: Array performance in synthetic data 3.4.1 Performance optimized design in water flow model 3.4.2 Performance optimized design in checkerboard Part IV: Practical aspects for data acquisition 3.5.1 Injection time cussion Part I: Spread and spacing	11 12 15 16 16 18 18 18 29
	3.1 3.2 3.3 3.4 3.5 Disc 4.1 4.2	Description of the case study. Part I: Spread and spacing Part II: Array design Part III: Array performance in synthetic data 3.4.1 Performance optimized design in water flow model. 3.4.2 Performance optimized design in checkerboard. Part IV: Practical aspects for data acquisition. 3.5.1 Injection time. cussion Part I: Spread and spacing. Part II: Array design.	11 12 15 16 16 18 18 18 29 29
	3.1 3.2 3.3 3.4 3.5 Disc 4.1 4.2 4.3	Description of the case study. Part I: Spread and spacing Part II: Array design Part III: Array performance in synthetic data 3.4.1 Performance optimized design in water flow model 3.4.2 Performance optimized design in checkerboard Part IV: Practical aspects for data acquisition 3.5.1 Injection time cussion Part I: Spread and spacing	111 12 15 16 16 18 18 18 29 29 30
4	3.1 3.2 3.3 3.4 3.5 Disc 4.1 4.2 4.3 4.4	Description of the case study. Part I: Spread and spacing Part II: Array design Part III: Array performance in synthetic data 3.4.1 Performance optimized design in water flow model 3.4.2 Performance optimized design in checkerboard Part IV: Practical aspects for data acquisition 3.5.1 Injection time cussion Part I: Spread and spacing Part II: Array design Part III: Array performance	111 12 15 16 16 18 18 18 29 29 30

Acknowledgements

I would like to thank Prof. dr. ir. Timo Heimovaara for giving me the opportunity to work in such an innovative project and for his invaluable advice.

I am also grateful to my daily supervisor, Andre van Turnhout, for his guidance and for encouraging me to think critically. Working with him during this eight months involved a lot of hard work, rain and sun, but it has been a lot of fun and I have learned a lot from him.

A very special gratitude to the people from the Geo-Engineering department, friends and family.

I am grateful to my sister, Anita, for her moral support and for bringing happiness to my life.

And finally, I must express my gratitude to my mother for providing me with her love and wisdom. Without her, this work would not have been possible.

Juan Chavez Olalla Delft, July 2017

1

Introduction

1.1. Justification

Traditional landfills have a emission potential which requires eternal after care in order to prevent release of contaminants to the environment. Emission potential has environmental, economical, and ethical implications. For this reason, the Dutch Sustainable Landfill Foundation (DSLF) aims to evaluate the effects of sustainable landfill methodologies at existing landfills in the Netherlands [1]. This is, it aims to apply methodologies to reduce or eliminate emission potential of contaminants in leachate and gases in the short term. For that purpose, aeration will be implemented in order to stimulated aerobic degradation in three experiments: one in the Wieringermeer and two in the Braambergen landfills. There are two main goals of the experiment. First, to evaluate the effects of aeration as a measure of stabilization of existing landfills. Second, to establish a generic procedure for application of aeration in other landfills.

Direct sampling of solid waste is not suitable to evaluate degradation of the refuse because of the large scale of the experiments and their highly heterogeneous nature. Instead, Key Performance Indicators (KPI) are monitored, so that an insight of the degradation process is obtained. Among the most relevant KPI are leachate flux, leachate quality, temperature, and moisture content. These indicators give a quantitative insight into the process of degradation by means of numerical models. A numerical model is sought that gives a response close to the observed response (KPI) and thus insight into the model states such as the emission potential. Such models have high degree of uncertainty because of the limited data available, for example, sampling values of KPI. Indeed, in the model developed specifically for the aforementioned experiments to estimate the emission potential [2], the water content plays a paramount role; nevertheless, information is scarce. Thus, the water content is a calibrated parameter rather than input data as it would be preferred to be because the model strongly depends on it.

Landfill bodies are prone to preferential fluid flow [3] which is difficult to assess deterministically. For such complex systems, it seems practical to account for preferential flow in terms of stochastic distribution of retention times. Thus, the total amount of water is discretized and each discrete element is classified into mobile or immobile according to the time elapsed for them to leave the system. Indeed, volumes of water with retention time larger than certain threshold are considered immobile; otherwise mobile. In the model of van Turnhout [2] solute masses are transported from the immobile water volume to the mobile through diffusion and from there, solute masses leave the system according to the retention time of the mobile water volume they are in. This preferential-flow behavior is one of the main concerns for applying aeration as a measure of stabilization. This is because air flow might not cover the extension of the waste body, yet it might show an apparent clean up in the short term. Nevertheless, concentration of contaminants in leachate would rise as soon as contaminants are diffused to the mobile phase. Therefore, in order to assess whether waste clean up is apparent or real, the water content of the waste body has to be characterized, so that the results are interpreted in a robust manner through model states.

1. Introduction

Electrical Resistivity Tomography (ERT) is a promising method to characterize the water content because resistivity is strongly correlated to moisture content. Moreover, ERT provides three-dimensional information which is preferred compared to direct sampling which is zero dimensional. The geophysical method consists in deriving a resistivity field from inversion of apparent resistivity values measured with several electrode configurations. For this purpose, a grid of borehole electrodes was installed with the aeration infrastructure of each of the three aforementioned experiments. This grid of borehole electrodes combined with surface electrodes is to be used to map electrical resistivity of the waste body. Although mapping water content is the final goal of the ERT monitoring program, it is crucial first to map as accurately as possible the resisitivity. Once reliable information about resistivity is obtained, mapping of water content is possible. ERT has been used for a wide range of applications such as environmental, hydrological, archaeological, mineral, and hydrocarbon exploration. However, the method shows significant discrepancies when applied to synthetic data or when compared with accurate prior information [4]. Indeed, there is an inherent limitation of the method because of the type of equation that describes the physical problem. Consequently, it is crucial to get the best of the method. This can be achieved by a proper grid design, array design, and considering the effect of operational aspects in data acquisition.

1.2. Research question

Given a base grid of borehole electrodes, what is the optimum survey strategy to monitor electric resistivity?

This thesis will present a systematic approach (protocol) to find an optimum survey strategy. Optimum survey strategy is understood in this study as a balance between resolution, covered area, acquisition time, and data error. This is to be implemented in the monitoring program at the Wieringermeer and Braambergen landfills. The main elements of this protocol are the selection of grid spread and electrode spacing, experimental array design, synthetic array testing, and practical aspects for data acquisition.

2

Methodology

2.1. General approach

The protocol formulated in this study is meant to make specific guidelines for monitoring resistivity in landfills. These specific guidelines are derived from general guidelines found in literature for geophysics and ERT. The protocol consists of four concatenated parts. In part one, grid spread and electrode spacing are defined. The objective criteria to evaluate grid designs are the model resolution and the covered area by the designs. In part two, survey array is designed by choosing four-electrode configurations in a systematic manner, i.e., configurations are ranked according to their influence in the model resolution. In part three, the performance of the array design is evaluated with synthetic data. This is done in terms of one to one comparison between true and inverted resistivity. In part four, the influence of practical aspects on the data error is studied. Finally, the survey strategy is formulated from the previous analysis.

2.2. Part I: Spread and spacing

The survey design in this study aims to retrieve high resolution information while covering the largest possible area. Since the design is constrained by the number of electrodes that can be used in a single survey, these two criteria are in contradiction. For instance, in order to retrieve information with higher resolution, more electrodes are needed, but in turn the covered area is smaller. Therefore, a trade-off between these two criteria, resolution and area, is to be found. In order to do so, several design alternatives are evaluated in terms of the two objective criteria, namely resolution and covered area. This is done until a set of designs (Pareto set) is found for which there is no other design that would improve one criteria without deteriorating the other criteria [5] (Figure 2.1). From the Pareto set, the most suitable design is chosen. The construction of a Pareto set is computationally expensive; thus, a limited number of operational-feasible designs are evaluated. In the subsequent subsections, it is explained how resolution and covered area are calculated.

2.2.1. Model resolution

In geophysics, model parameters are estimated, so that when an appropriate physics-based model is applied to those parameters, the response is similar, within an error range, to the measured response. An example of parameter estimation (inversion) is least squares fitting in which the square error between fitting points (measured data) and a equation output (model response) is minimized. A qualitative idea of resolution is drawn from this illustration. If there are more data points than model parameters to be fitted, then the resolution of each of the model parameters is one. In ERT, the inverse problem maintains certain similarities with the least square fitting problem. Nonetheless, some differences are noticeable such as the model response is a non-linear function of the model parameters. Also, there are an infinite number of model responses that satisfy the measured response. Thus, in order to solve the inverse problem, regularization is applied. For instance, a type of regularization is to

4 2. Methodology

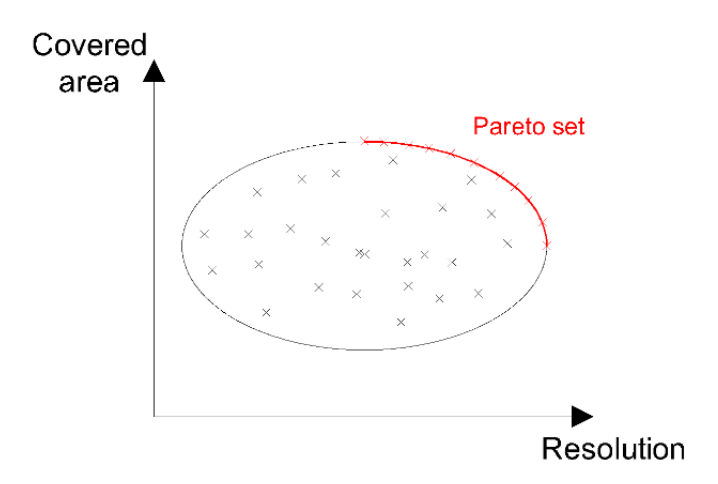


Figure 2.1: Pareto set (red line).

assume the distribution of parameters is smooth or the parameters are close to a fixed value. However, these assumptions influence the reliability of the inverted parameters. Thus, it is desired that the model parameters are estimated from the measured data. In qualitative terms, a model parameter that is completely estimated from the measured data has a resolution of one whilst a model parameter that is partly estimated from the data and partly from the regularization has a resolution lower than one. Formally, the model resolution (Equation 2.1) comes from the weighted damped least squares solution of the linearized inverse problem [6]:

$$R = (G^T G + C)^{-1} G^T G (2.1)$$

where G and C are the sensitivity and regularization matrices, respectively (explained bellow).

In the inversion process, the resistivity field is discretized and the resistivity of the discrete elements are the model parameters to solve for. Consequently, the model resolution is a square matrix of size equal to the number of model parameters. Each row of the resolution matrix contains information about the resolvability of a specific model parameter. For instance, the ith row of the resolution matrix contains information about the resolvability of the ith model parameter, i.e., how much each model parameter influence the solution of a specific inverted model parameter. Therefore, the diagonal elements of the resolution matrix say how a inverted model parameter influences itself. The diagonal is generally used as an indicator of resolvability rather than the complete matrix. The structure of the resolution matrix is shown in Figure 2.2. In this matrix, i and j go from 1 to the number of model parameters.

$$R_{ij} = \begin{bmatrix} R_{11} & R_{12} & \dots & R_{1j} \\ R_{21} & R_{22} & \dots & R_{2j} \\ \vdots & \vdots & \ddots & \vdots \\ R_{i1} & R_{i2} & \dots & R_{ij} \end{bmatrix}$$

Figure 2.2: Structure of the resolution matrix.

The model resolution is composed of the sensitivity matrix G (Equation 2.2) and the regularization matrix C. C contains the damping factor, a priory information and type of constraint.

$$G_{i,j} = \frac{\partial (V_i)}{\partial (\rho_i)} \tag{2.2}$$

The sensitivity matrix is composed of the partial derivatives of the model responses with respect to

the model parameters [7]. This matrix has as many rows as configurations and as many columns as model parameters. The structure of the sensitivity matrix is shown in Figure 2.3. In this matrix i goes from 1 to the number of configurations and j goes from 1 to the number of model parameters.

$$G_{i,j} = \begin{bmatrix} \frac{\partial V_1}{\partial \rho_1} & \frac{\partial V_1}{\partial \rho_2} & \cdots & \frac{\partial V_1}{\partial \rho_{nm}} \\ \frac{\partial V_2}{\partial \rho_1} & \frac{\partial V_2}{\partial \rho_2} & \cdots & \frac{\partial V_2}{\partial \rho_{nm}} \\ \vdots & \vdots & \ddots & \vdots \\ \frac{\partial V_{nc}}{\partial \rho_1} & \frac{\partial V_{nc}}{\partial \rho_2} & \cdots & \frac{\partial V_{nc}}{\partial \rho_{nm}} \end{bmatrix}$$

Figure 2.3: Structure of the sensitivity matrix.

2.2.2. Covered area

The covered area in a single survey is determined by the spatial distribution of the electrodes. When the area of investigation is large, a principal direction is defined in which electrodes are oriented. Multiple lines are reproduced with the same orientation and at a fixed separation. This is done until all the electrodes are used. The transverse separation of the electrode lines is determined in this study by following generic guidelines found in literature [8]. Therefore, array design and data acquisition are two-dimensional because of the limited number of electrodes available; nevertheless, the inversion can be three-dimensional. The covered area is calculated as

$$Area = L * t * n, \tag{2.3}$$

where L is the longitudinal spread, t is the transverse separation between lines, and n is the number of lines covered by the available number of electrodes.

2.3. Part II: Array design

Four-electrode configurations are most commonly used in ERT because of operational convenience and resolution properties. Using pole-pole or pole-dipole configurations present some disadvantages such as the need of a far electrode in order to guarantee pole-pole conditions or low resolution compared to four-electrode configurations [9]. Traditional array design has been limited to the use of standard arrays such as dipole-dipole, Schlumberger and Wenner arrays. Nevertheless, for special grid geometries, standard arrays are cumbersome to implement. Moreover, the information content of data collected using traditional arrays is low compared to the total information that can be collected with four-electrode configurations. An obvious alternative to exploit the ERT method would be to collect data using all possible four-electrode configurations, comprehensive data set. However, this becomes unpractical in terms of survey time and computational power even for small number of electrodes. This is illustrated by the set of all non-reciprocal configurations, comprehensive set, available which scales with the fourth power of the number of electrodes [10]

$$n_{comprehensive} = \frac{n(n-1)(n-2)(n-3)}{8}.$$
 (2.4)

For this reason, a robust approach is needed to design arrays by choosing the best four-electrode configurations out of the comprehensive set. The best configurations are those who produce the highest increment in the model resolution. Several systematic approaches to select configurations are found in the literature such as the compare R method [11] and the goodness function [12]. The chosen approach used in this study is the goodness function because is the less expensive in terms of computing time. In multiple channel acquisition systems, data can be complemented by filling empty commands with non-standard configurations. Thus, the goodness function used in this study was modified in order to choose the best configurations while filling empty commands at the same time.

6 2. Methodology

2.3.1. Goodness function

This method aims to increase the values of the diagonal elements of the resolution matrix. The goodness function is expressed as follows:

$$GF_{i} = \sum_{i=1}^{nm} \frac{G_{ij}^{cand}}{G_{j}^{sum}} (1 - \frac{R_{jj}^{base}}{R_{jj}^{comp}})$$
 (2.5)

where nm is the number of model cells, G_{ij}^{cand} is the sensitivity of the candidate set of configurations, G_{j}^{sum} is a normalization factor, R_{jj}^{base} and R_{jj}^{comp} are the diagonals of the base and comprehensive model resolution, respectively. A more comprehensive description of the goodness function is found in Stummer $et\ al.\ [12]$. Equation 2.5 ranks configurations according to their sensitivity (Equation 2.2) and their effect on the model resolution. Such that, configurations that are sensitive to model parameters with low resolution have a higher ranking.

The complete implementation of the goodness function is described in the following algorithm and illustrated in Figure 2.4:

- 1. Compute the threshold resolution R_{comp} of the comprehensive data set
- 2. Choose a base set of configurations dipole-dipole
- 3. Compute the resolution R_{hase} of the base data set
- 4. Define the candidate set of configurations by removing from the comprehensive data set the base set
- 5. Carry out orthogonality check (dot product) between the sensitivity of the candidate set and the base set. Then, discard configurations whose dot product is larger than a predefined threshold
- 6. Apply the goodness function to the remaining candidate configurations
- 7. Choose best ranked configurations and add them to the base set
- 8. Fill empty commands with the best ranked configurations and according to the working principle of the acquisition system being used
- 9. Repeat from step three until the array design is complete

2.4. Part III: Array performance in synthetic data

2.4.1. Water flow model

A geohydrological model, which is representative of landfill conditions, is used for synthetic data generation. This is a two-phase gas-liquid fully coupled flow model. It was implemented in COMSOL Multiphysics to study aeration mechanics in landfills [13] and will be used as a source of synthetic data. This model assumes a linear change of porosity in depth going from high on top to low at the bottom. Neumann boundary conditions are given for water flow and Dirichlet for air flow at the top. At the bottom, Robbins boundary conditions are applied for water flow and Dirichlet for air flow. The infiltration rate of water, top boundary condition, is changed in order to analyze two possible scenarios, namely wet and dry. The steady state solution of the differential equations shows the water saturation going from low at the top to high at the bottom. The water content goes from high at the top to low at the bottom (see Figure 2.5) which is a consequence of the porosity profile.

From this model, the volumetric water content is correlated to resistivity by means of Archie's law:

$$\rho = a\rho_1 \theta^{-m} \tag{2.6}$$

where ρ_1 is the electrical resistivity of the leachate, θ the volumetric water content, and m and n are empirical parameters. From Grellier *et al.* [14] a=1, m=2.5, and ρ_1 is chosen to be 2 ohm-m in order to fit the resistivity in the range observed in the field.

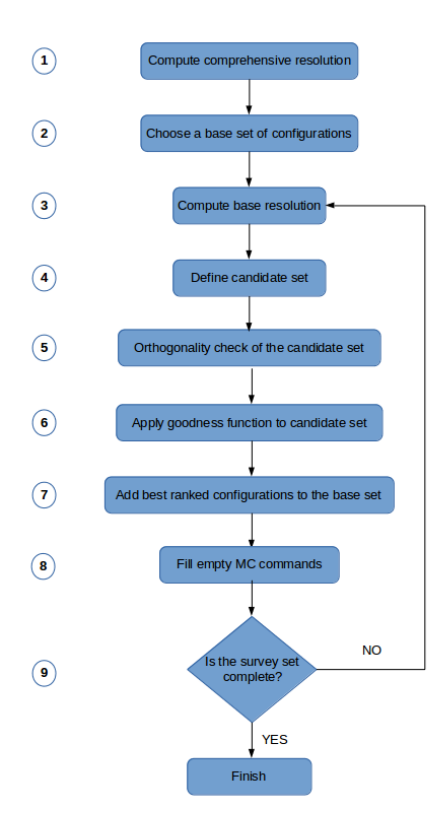


Figure 2.4: Diagram for experimental design.

2.4.2. Checker board model

Since the flow model shows a smooth transition of resistivities and the inversion algorithm uses smoothness type of constraint, the inverted model parameters are in agreement with the true model parameters (flow model). Therefore, a checkerboard type of model is crucial in order to make a fair assessment of the array design, for smoothness constraint is not in agreement anymore with the true resistivity field (checkerboard model). This model consists of a background resistivity similar to that obtained in pre-design surveys. Circular anomalies with high resistivity are added to the background model also in accordance to the anomalies found in pre-design surveys (Figure 2.6).

2.5. Part IV: Practical aspects for data acquisition

2.5.1. Injection time

The resistivity system (Syscal Pro, Iris Instruments) allows the use of different injection times. The injection time is preferred to be short in order to reduce survey time. Nevertheless, using short injection time might lead to a faulty measurement in mediums prone to induced polarization because the voltage field is not stable [15]. Measurements with different injection times are taken and compared in order to determine a suitable injection time.

2.5.2. Polarization effects

Data error can be estimated from repeated measurements, yet a better estimator of data error is the reciprocal error [15]. Reciprocal measurements imply longer acquisition time compared to repeated measurements which is not desired. Therefore, a strategy is sought to reduce reciprocal errors, so that a good estimator of data error would be obtained with repeated measurements only. Reciprocal errors can be significantly reduced by reducing electrode polarization [16]. That is, rearrange the injection sequence in such a way that the longest time is elapsed for an electrode to work as potential electrode after it worked as current electrode.

8 2. Methodology

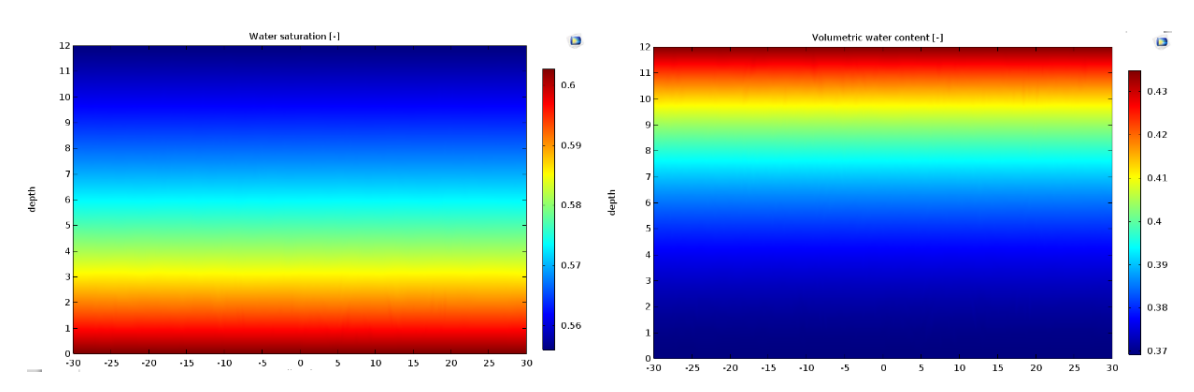


Figure 2.5: Water saturation (left) and water content (right).

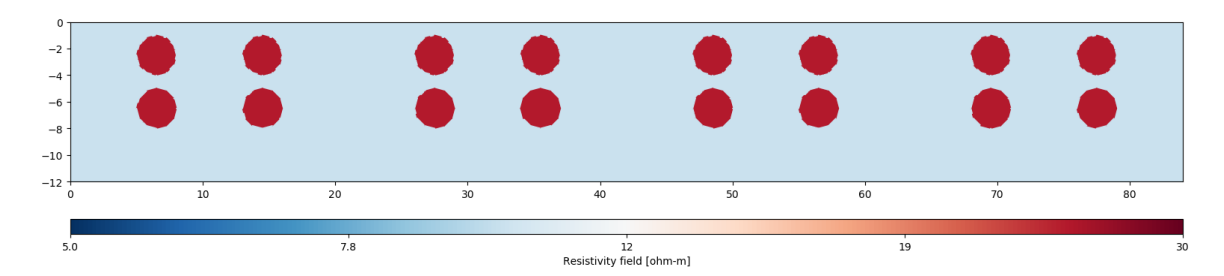


Figure 2.6: Checkerboard model.

First, a brief discussion on the working principle of a multiple channel acquisition system is presented. A command with M channels is formed by two injection electrodes (C) and M+1 potential electrodes P. For example, command i is formed as follows:

$$C_{i1}, C_{i2}, P_{i1}, P_{i2}, P_{i3}, ..., P_{i(M+1)}$$
.

Then, the M measurements of command i are:

$$C_{i1}C_{i2}P_{i1}P_{i2}$$
, $C_{i1}C_{i2}P_{i2}P_{i3}$,..., $C_{i1}C_{i2}P_{iM}P_{i(M+1)}$.

The problem of rearranging commands can be formulated as a minimization problem. The objective function is defined as a cost function [16]

$$c = \sum_{i=1}^{n} \frac{1}{d_i},\tag{2.7}$$

where $d_i = j - i$ and j is the first subsequent command containing a potential electrode that was used as a current electrode in the ith command. Table 2.1 illustrates how the cost is calculated for a hypothetical case of a ten-channel acquisition system and five commands.

i	C1	C2	P1	P2	Р3	P4	Р5	Р6	P7	P8	P9	P10	j	d=j-i	1/d
1	1	4	2	3	5	6	7	8	9	10	11	12	2	1	1
2	1	5	2	3	4	6	7	8	9	10	11	12	3	1	1
3	1	8	2	3	5	6	7	9	10	11	12	13	4	1	1
4	1	12	2	3	4	5	6	7	8	9	10	11	inf	inf	0
	•													С	3

Table 2.1: Cost function calculation

A simulated annealing algorithm is applied following Wilkinson *et al.* [16] in order to minimize the cost function. The global optimization toolbox of Matlab was used for this purpose.

2.5.3. Geometrically unstable configurations

The comprehensive data set contains configurations whose geometric factor is highly sensitive to electrode positions. This type of configurations are not convenient for data acquisition, for electrode positions are in practice rather inaccurate. Geometrical sensitivity is reflected on field data as high or negative values of apparent resistivity [17]. The methodology presented in Wilkinson *et al.* [16] is used in order to filter out these configurations. Unstable configurations are those whose geometric relative error is larger than five [16]

$$R_E = s/K, (2.8)$$

where *s* is the sensitivity of the geometric factor to errors in the positions:

$$s^{2} = \left(\frac{\partial K}{\partial A}\right)^{2} + \left(\frac{\partial K}{\partial B}\right)^{2} + \left(\frac{\partial K}{\partial M}\right)^{2} + \left(\frac{\partial K}{\partial N}\right)^{2},\tag{2.9}$$

where $\partial K/\partial A$, $\partial K/\partial B$, $\partial K/\partial M$, $\partial K/\partial N$ are the sensitivities of the geometric factor to electrode positions A, B, M, and N, respectively:

$$\left(\frac{\partial K}{\partial A}\right)^2 = \left(\frac{\partial K}{\partial x_A}\right)^2 + \left(\frac{\partial K}{\partial y_A}\right)^2 + \left(\frac{\partial K}{\partial z_A}\right)^2; \tag{2.10}$$

$$\left(\frac{\partial K}{\partial B}\right)^2 = \left(\frac{\partial K}{\partial x_B}\right)^2 + \left(\frac{\partial K}{\partial y_B}\right)^2 + \left(\frac{\partial K}{\partial z_B}\right)^2; \tag{2.11}$$

$$\left(\frac{\partial K}{\partial M}\right)^2 = \left(\frac{\partial K}{\partial x_M}\right)^2 + \left(\frac{\partial K}{\partial y_M}\right)^2 + \left(\frac{\partial K}{\partial z_M}\right)^2; \tag{2.12}$$

$$\left(\frac{\partial K}{\partial N}\right)^2 = \left(\frac{\partial K}{\partial x_N}\right)^2 + \left(\frac{\partial K}{\partial y_N}\right)^2 + \left(\frac{\partial K}{\partial z_N}\right)^2,\tag{2.13}$$

where x, y and z are the positions of the electrodes and Δx , Δy and Δz are the position errors. The geometric factor K is:

$$K = \frac{4\pi}{\frac{1}{r_{AM}} - \frac{1}{r_{AN}} - \frac{1}{r_{BM}} + \frac{1}{r_{BN}} + \frac{1}{r_{A/M}} - \frac{1}{r_{A/M}} - \frac{1}{r_{B/M}} + \frac{1}{r_{B/M}} + \frac{1}{r_{B/N}}} = \frac{4\pi}{H},$$
 (2.14)

where r_{ij} is the distance between electrode i and j and the positions of the image wells are related to the positions of the real wells xi' = xi, yi' = -yi and zi = zi.

Results

3.1. Description of the case study

The Brambergen landfill close to Almere, The Netherlands was chosen as a case study. The base grid of electrode is composed of thirty five boreholes. Each borehole contains seven electrodes with separation of two meters. The grid of boreholes is composed of seven rows and five columns. The separation between boreholes is twenty one meters, so the total area covered by the grid of electrodes is approximately $10,000m^2$. Figure 3.1 shows the base grid of electrodes. The waste body of the landfill is encapsulated by a bottom liner at fourteen meters depth and a two-meter soil cover. The largest changes in resistivity due to aeration are expected in the waste body (two to twelve meter depth), so this depth range is defined as the target. The large spacing between boreholes makes unfeasible to only use the base grid of boreholes, so a smaller sub grid of boreholes is sought which combined with surface electrodes is optimum for data acquisition.

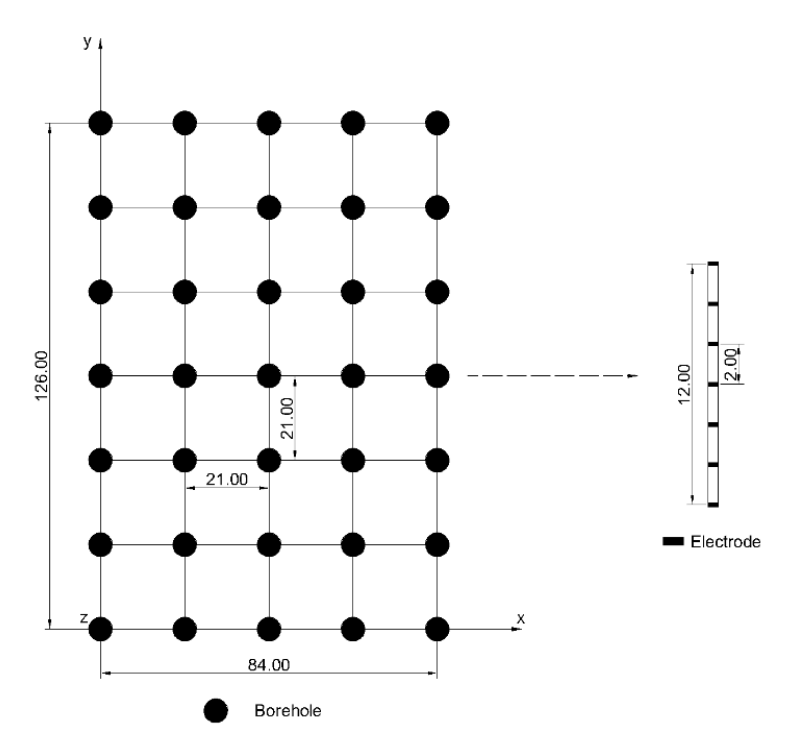


Figure 3.1: Base grid of borehole electrodes.

It is desired in this study to retrieve three-dimensional information of the resistivity field of the landfill. This can be achieved by taking measurements in all possible directions. Nevertheless, this is

12 3. Results

only possible when the grid of electrodes covers completely the extension of the survey area. This seldom happens, for the number of electrodes and their separation is restricted. Alternatively, three-dimensional information can be obtained by dividing the total survey area in sub grids and roll along them. These rectangular sub grids have considerably longer electrode lines in x than in y direction. Therefore, data is collected along these long lines only. The transverse separation between long lines is preferred to be less than twice the electrode separation [8] in the long direction. Based on this general rule, the transverse separation is chosen as 5.25m. This separation would allow to fit three lines between boreholes if there would be enough electrodes available. Also, it is less than two times the maximum electrode separation (3.0m). In order to truly retrieve three-dimensional information, representative data along the y direction has to be collected in addition to that in the x direction. In order to do so, the survey direction has to be rotated, so the longer lines are oriented in y direction. However, data collected along the x direction can be an indicator of three-dimensional structures although not as good as data collected in both x and y direction. In any case, a grid has two type of electrode lines. That is, lines with surface and borehole electrodes (SF-BH in Figure 3.2) and lines with surface electrodes only (SF in Figure 3.2).

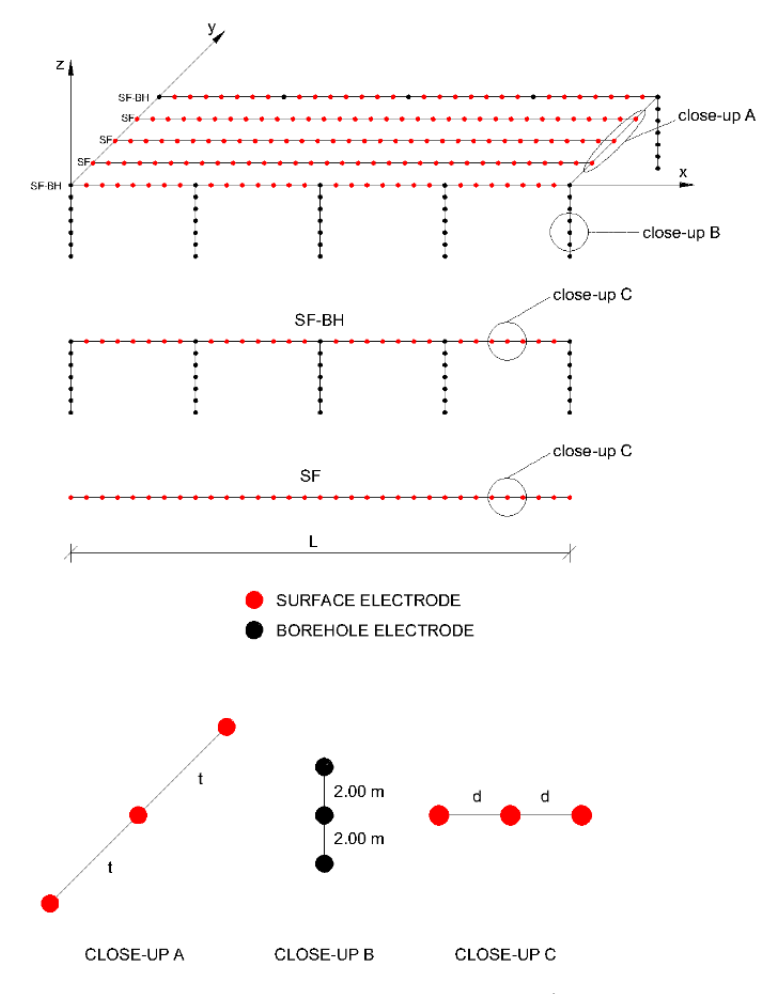


Figure 3.2: Data acquisition approach.

3.2. Part I: Spread and spacing

Twenty grid designs were evaluated in order to find a grid with an optimum spread and spacing. Optimum in this context means that the largest extension is covered whilst resolution is kept high. This optimum grid is to be used in a subsequent step for array design, that is, choosing four-electrode configurations for data acquisition. Grid designs were evaluated in terms of covered area (Equation

2.3) and relative average resolution (relative with respect to the maximum of the twenty designs). The average resolution was calculated as the average of the diagonal elements of the model resolution matrix (Equation 2.1). The average was calculated for the 'SF' lines only (Figure 3.2), for they are the most unfavourable in terms of resolution. The sensitivity matrix (Equation 2.2) was calculated for the comprehensive set of configurations (Equation 2.4). Although for data acquisition the comprehensive set of configurations is unfeasible, during the array-design stage, a smaller set of configurations can be found, so that the information content is comparable to that of the comprehensive data set [11, 12]. The regularization strength was approximated by $C = \lambda I$ where $\lambda = 2.5e - 6$ following Wilkinson et al. [11]. Detailed information of the grid design alternatives evaluated in this section is summarized in table 3.1.

Table 3.1: Design alternatives

Design	BH-SF	SF	Lines	Elec	d	L	t	A	relR
1	2	6	8	200	1.00	21.00	5.20	873.60	0.751
2	3	9	12	216	1.50	21.00	5.20	1310.40	0.448
3	4	11	15	213	2.10	21.00	5.20	1638.00	0.240
4	5	12	17	213	2.60	21.00	5.20	1856.40	0.164
5	5	14	19	212	3.00	21.00	5.20	2074.80	0.126
6	1	3	4	190	1.00	42.00	5.20	873.60	0.912
7	2	4	6	210	1.50	42.00	5.20	1310.40	0.598
8	2	6	8	204	2.10	42.00	5.20	1747.20	0.352
9	2	8	10	206	2.60	42.00	5.20	1965.00	0.265
10	2	9	11	201	3.00	42.00	5.20	2184.00	0.217
11	1	2	3	216	1.00	63.00	5.20	982.80	0.980
12	1	3	4	196	1.50	63.00	5.20	1310.40	0.656
13	2	3	5	203	2.10	63.00	5.20	1638.00	0.394
14	2	4	6	198	2.60	63.00	5.20	1965.60	0.311
15	2	5	7	202	3.00	63.00	5.20	2293.20	0.261
16	1	1	2	200	1.00	84.00	5.20	873.60	1.000
17	1	2	3	201	1.50	84.00	5.20	1310.40	0.685
18	1	3	4	194	2.10	84.00	5.20	1747.20	0.429
19	1	3	4	162	2.60	84.00	5.20	1747.20	0.333
20	2	3	5	205	3.00	84.00	5.20	2184.00	0.279

Nomenclature table 3.1:

SF-BH: Number of lines containing both borehole and surface electrodes

SF: Number of lines containing surface electrodes only

Lines: Total number of lines in the grid Elec: Total number of electrodes in the grid

d: Separation between surface electrodes in x direction

L: Spread of the grid in x direction

t: Transverse separation of electrode lines (y direction)

A: Covered area by the grid relR: Relative average resolution

The Pareto set is built (red line in Figure 3.3) from the evaluation of several grid alternatives. This set defines the boundary for grid performance, so at this boundary it is not possible to improve one objective without damaging the other. On the other hand, designs that are not part of the Pareto set (blue crosses in Figure 3.3) have to be discarded, for there are others that perform better in terms of area and resolution. Figure 3.3 shows that the resolution might be significantly affected by the chosen grid. Indeed, a poorly chosen grid might lead to low resolution data. Therefore, the Pareto set approach is effective for exploiting the potential of the geophysical method. Many grids should be used in order to build a reliable Pareto set. In this study, 20 grids were analyzed in order to cover a representative portion of the available grid options. Nonetheless, more designs could be evaluated in

14 3. Results

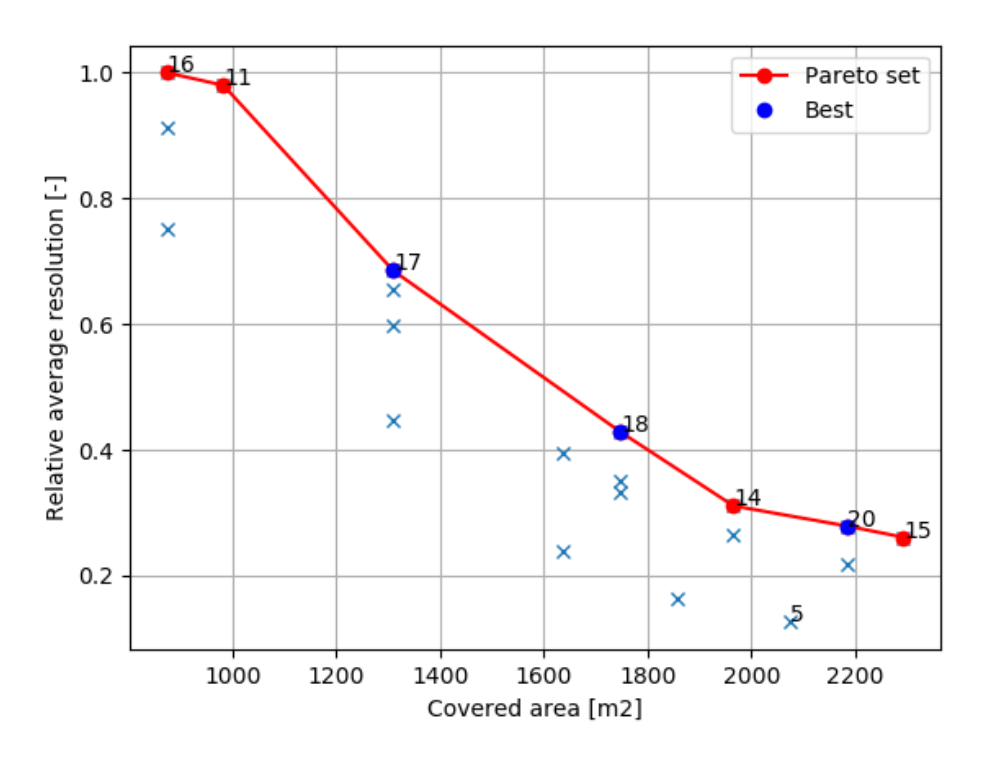


Figure 3.3: Pareto set.

h]

an attempt to extend the limits of the Pareto set. For example, designs with variable electrode spacing could reach this goal. Indeed, Wagner *et al.* [18] showed that by allowing variable electrode separation, the resolution is increased and electrodes are more efficiently used. Nevertheless, the approach of the aforementioned study was applied to borehole electrodes whose position is less prone to error. Meanwhile, for the intended application of this study, positioning is not as accurate and the operation has to carried out every time a survey is carried out, which is unpractical. Therefore, the 20 grids evaluated are representative of the design options available. Grid designs that constitute the Pareto set are taken for further analysis, so that a final design choice is made. These designs are 11, 14, 15, 16, 17, 18, 20 (see Table 3.1 and Figure 3.3 for details). Additionally, design number 5 was also taken for further analysis, so that the possibility of taking transverse measurements is assessed.

An additional analysis is carried out for the previously selected designs. They are evaluated in terms of vertical resolution, which is the average resolution with respect to depth. The values of the vertical resolution were normalized with respect to the highest value which corresponds to that of the upper part in design 16. The vertical resolution of the designs in the Pareto set is plotted Figure 3.4. The first conclusion from Figure 3.4 is that grids with small spread, such as that of design 5, have extremely low resolution, especially at the target depth. As a result, transverse measurements do not contain relevant information, so they are not considered for array design. The highest vertical resolution is found in grids 11 and 16, but the coverage of these grids is extremely low, so they are discarded. On the other hand, grids 14, 15, and 20 show the largest coverage, but the lowest vertical and total resolution, with grid 14 as the best performing in this matter. Grids 17 and 18 are a trade-off between resolution and area. The vertical resolution of grid 17 is markedly higher than that of grid 18 in the first two meters. Nevertheless, the target depth is from two to twelve meters, in which case both grids shows similar behavior, but grid 18 covers a larger area. Therefore, grid 18 is selected for subsequent array design. In brief, selecting a final grid is a subjective choice which depends on the specific needs of the user.

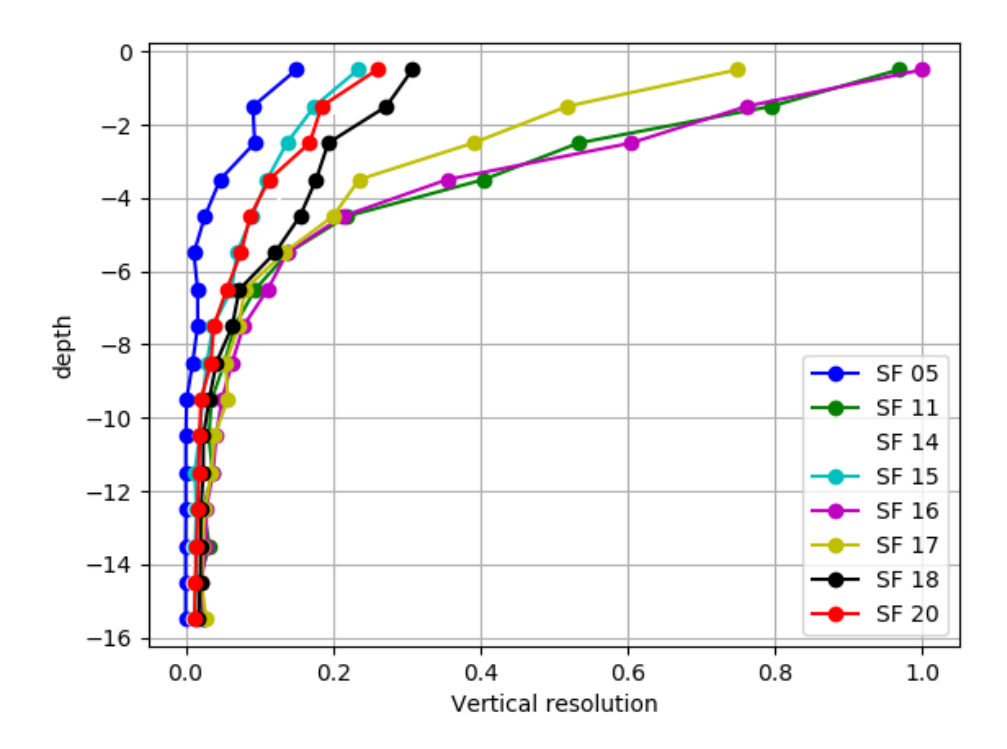


Figure 3.4: Vertical resolution of the designs in the Pareto set and design 5.

3.3. Part II: Array design

Grid number 18 is selected for array design although the approach used in this stage is applicable to any grid of electrodes. Grid 18 has four parallel lines along the x direction with spread of 84 meters. One of those lines is of the type SF-BH with five boreholes, whilst the other three lines are of the type SF (Figure 3.2). Both type of lines are identical, except that the SF-BH line has additional buried electrodes. The SF-BH line has 71 electrodes and the SF lines have 31 electrodes. Electrodes in the x direction are spaced x0.1 m buried electrodes are spaced x0.2 m and the separation in the x1 direction of the lines is x2.2 m. In order to cover the survey extension the roll along technique has to be applied six times in the x3 direction. In summary, two type of arrays are designed SF-BH and SF. An SF array is designed with the goodness function (Equation 2.5). On the other hand, an SF-BH array is designed by using the SF array as base and then adding those configurations that are most sensitive in the inter borehole region. The reason for not using the goodness function for the SF-BH array is that a large number of installed borehole electrodes are either not well connected to the surrounding material or not functional. Therefore, the soundest approach is to use the optimized array that is completely functional (SF line) and use borehole information as additional information when it is reliable, but without risking the overall data acquisition.

The goodness function (Equation 2.5) is applied to the SF line in a homogeneous field according to the algorithm shown in Figure 2.4. The model resolution matrix (Equation 2.1) was approximated by using $C = \lambda I$ where $\lambda = 2.5e - 6$ following Wilkinson *et al.* [11]. The approximation is valid, for in comparing designs and configurations what is relevant is the relative value rather than the actual value of resolution. Indeed, this relative value tends to cancel out the effect of the regularization strength. The initial base set of configurations is a dipole-dipole and the candidate set of configurations is the comprehensive set which for 41 electrodes equals 303,810 configurations (Equation 2.4). The development of average resolution versus number of configurations added to the base set is shown in Figure 3.5. One percent of the comprehensive set, 3000 configurations, reaches 87 percent of the maximum achievable resolution. The remaining 99 percent of the configurations have little additional contribution to the resolution. The goodness function was modified for multiple channel acquisition,

3. Results

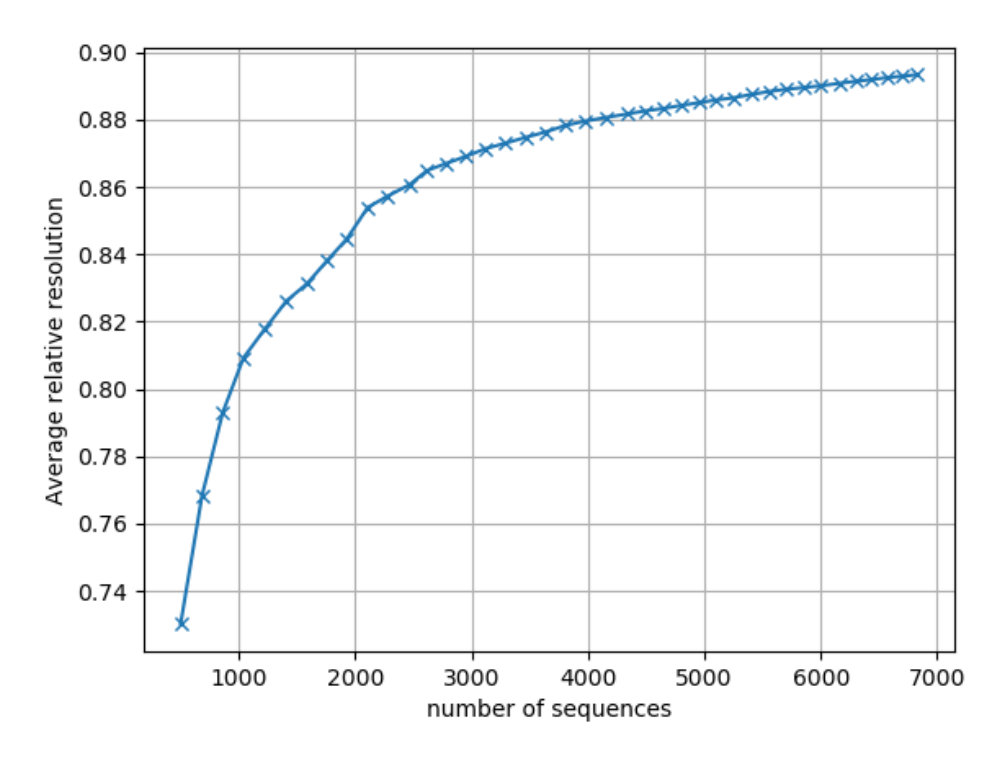


Figure 3.5: Average resolution development array with surface electrodes only.

so data acquisition in the field is considerable faster and more efficient than automatic filling of empty commands. The cut-off number of configurations has to be chosen by considering that a large number of measurements might be faulty and have to be discarded during data processing. For this reason, the first 3000 configurations are considered to be an appropriate amount for data acquisition.

An SF-BH array has the same configurations as an SF array with an additional 308 configurations which are a combination of borehole-to-surface and cross-borehole. These configurations are the most sensitive in the inter borehole region. The increment in resolution of the SF-BH line with respect to the SF line is assesses through a comparison between their vertical resolutions (Figure 3.6). This figure shows a significant increment in resolution, especially in the target depth which is from two to twelve meters. This increment in resolution is crucial to improve reliability of the lower part of the model which is the most problematic in terms of interpretation. By using the SF array as base instead of applying the goodness function directly, it is guaranteed that the borehole information has a positive effect on the data quality, for it can be used when good or discarded when faulty.

3.4. Part III: Array performance in synthetic data

3.4.1. Performance optimized design in water flow model

Two scenarios of water flow were analyzed, namely dry (Figure 3.7) and wet (Figure 3.12) with an infiltration rate of 0.036mm/h and 3.24mm/h, respectively. The resistivity field in the dry case shows a higher portion with high resistivities as opposed to what is observed in the wet scenario in which the portion which has high resistivity is smaller. On the other hand, the wet scenario shows a sharper profile of resistivities due to a sharper water content profile. The performance of the SF and SF-BH arrays were assessed in qualitative terms with the inverted models and in quantitative terms with the vertical recovery of resistivities.

For the dry scenario, the inverted model obtained with the SF array(Figure 3.8) shows a layered

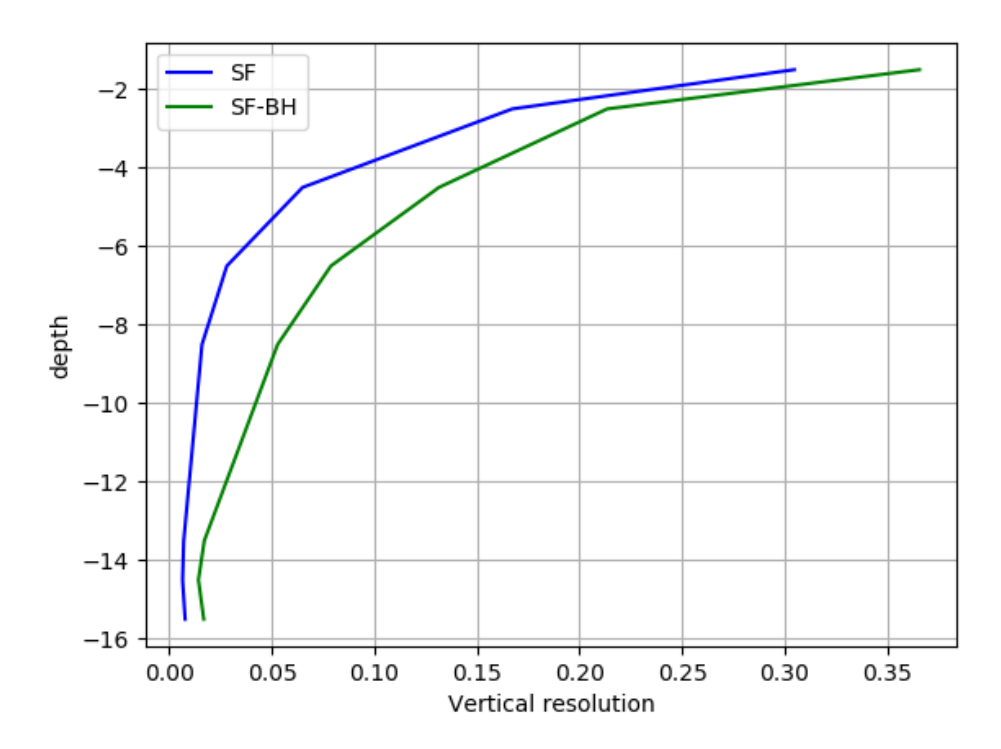


Figure 3.6: Comparison vertical resolution lines SF and SF-BH.

profile although it shows curved layers, which are not seen in the true model. The vertical recovery of resistivities (Figure 3.10) is identical to the true model up six meters depth for the SF line. After six meters depth, the vertical recovery starts to deviate from the true model although in absolute sense that deviation is not significant, but graphically it is noticeable. On the other hand, the inverted model obtained with the SF-BH array (Figure 3.9) shows a more truthful representation of the true model. Moreover, the SF-BH line recovers accurately the vertical resistivity field (Figure 3.11) even up to twelve meters depth and can reproduce the rather non-smooth behavior in the lower part.

For the wet scenario, the inverted model obtained with the SF array(Figure 3.13) shows a curved layered profile as seen in the dry case. The inverted model captures the change in size of the resistivity zones. The vertical recovery of resistivities (Figure 3.15) is identical to the true resistivity until eight meter depth for the SF line. After eight meter depth, the vertical recovery starts to deviate from the true model. Indeed, the wet scenario shows a non-smooth behavior in the lowest part which can not be recovered by the SF array. As seen in the dry case, the inverted model obtained with the SF-BH array (Figure 3.14) shows a more truthful representation of the true model. Moreover, the SF-BH line recovers accurately the vertical resistivity field (Figure 3.16), even the lower non-smooth part.

Finally, when comparing resistivity variation between the dry and wet scenario, the SF-BH array (Figure 3.18) shows a significantly better performance than the SF array (Figure 3.17). This comparison is crucial, for the implication is that the arrays are suitable for keeping track of vertical variations in moisture content which is one of the main goals of the monitoring program. Clearly, both the SF and the SF-BH arrays show a good performance to recover resistivity. This could be explained by the similarity between the smooth resistivity field and the smoothness regularization of the inversion algorithm. This similarity tends to average out inaccuracies. Nevertheless, the real resistivity field might have sharp contrasts in which the inversion algorithm does not perform well.

3. Results

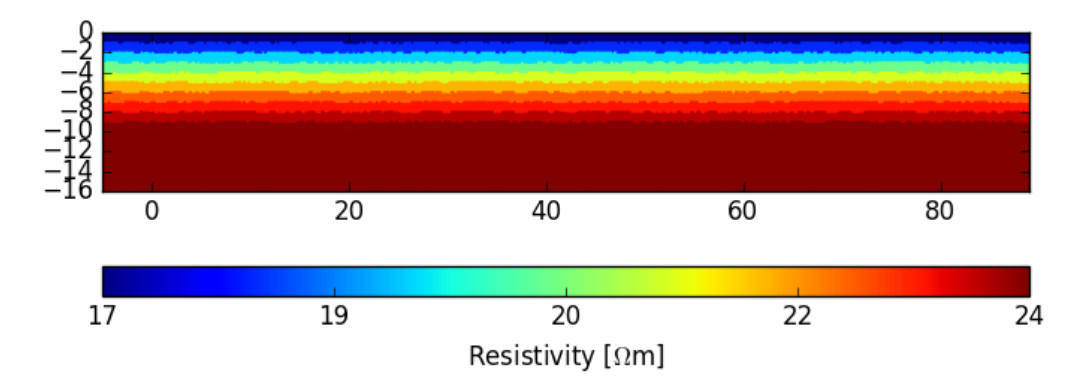


Figure 3.7: True resistivity field dry scenario.

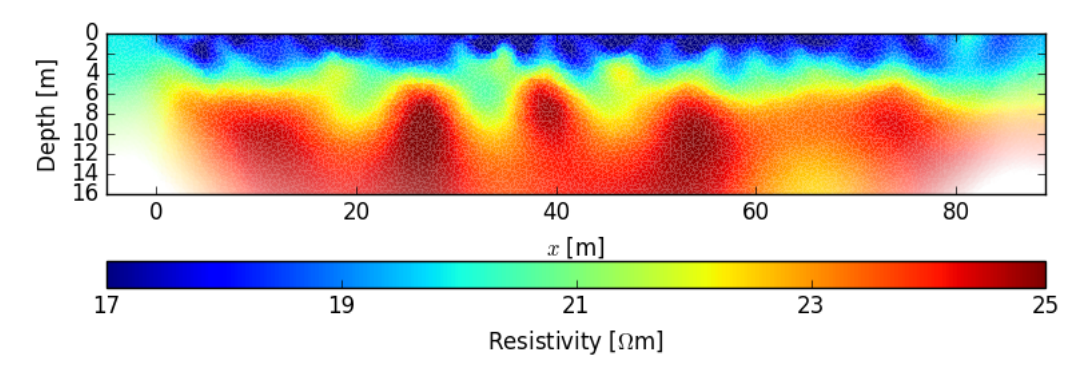


Figure 3.8: Inverted resistivity field dry scenario SF line.

3.4.2. Performance optimized design in checkerboard

A checkerboard type of model (Figure 3.19) is generated in order to test the array performance. The model consists of 16 circular anomalies with a resistivity of 25 ohm-m surrounded by a background resistivity of 10 ohm-m. First, the inverted image with the SF array (Figure 3.20) shows a good reconstruction of the upper row of anomalies, but the lower row does not appear in the reconstruction. Second, the inverted image with the SF-BH array (Figure 3.21) shows a good recovery of the upper row of anomalies, but a poor recovery of the lower row. Nevertheless, the lower row of anomalies is slightly better reconstructed which is seen as a white strip underneath each of the anomalies in the upper row. Therefore, the capability of the arrays to resolve a sharp resistivity field is limited even after optimization. This is a result of the type of regularization used for the data inversion and the low resolution in the lower region.

3.5. Part IV: Practical aspects for data acquisition

3.5.1. Injection time

A suitable injection time is sought which allows efficient data acquisition without compromising data quality. For this purpose, field measurements taken with a dipole-dipole array are analyzed for four injection times 8, 1, 0.5, and 0.25 seconds. The data is analyzed with histograms of data error (Figure 3.22) and apparent resistivity (Figure 3.23). Finally, a comparison of measured apparent resistivity with different injection times is carried out (Figures 3.24 and 3.25).

Data collected with injection time of 8s show the largest error. Similarly, data collected with injection time of 1s show also a large tail in the error histogram. Data with injection time of 250ms and 500ms show the smallest error. Histograms of apparent resistivity show more negative and unusually large values for injection times of 8s and 1s than for injection times of 500ms and 250ms although for 500ms there are less negative values of apparent resistivity. Most of the recorded negative apparent resistivity values show large error, but some negative apparent resistivity values shows low error.

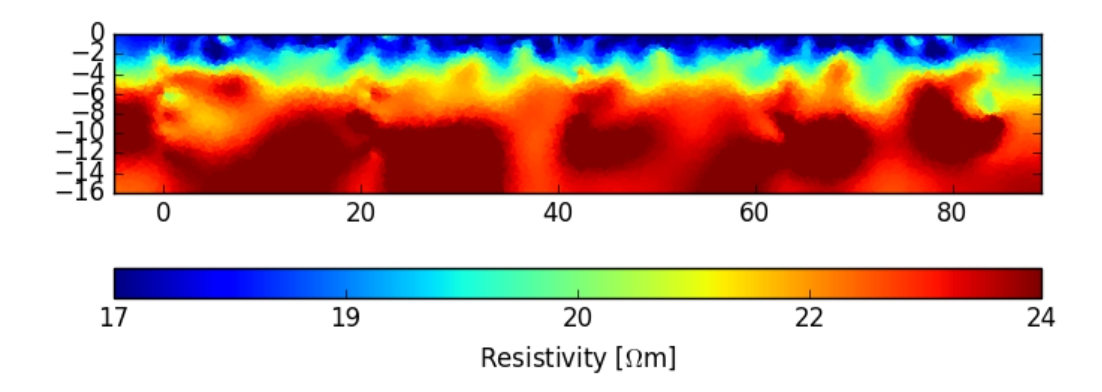


Figure 3.9: Inverted resistivity field dry scenario SF-BH line.

A comparison between the apparent resistivity is done in order to determine how reliable the measured data is and which injection time is the most suitable. This comparison is done for two cases; first, for data error less than 20 percent (Figure 3.24); second, for data error less than 5 percent (Figure 3.25). Although the data with error less than 20 percent show significantly more outliers than data with 5 percent error, 72 to 85 percent of the data can be used for inversion (table 3.2). Whereas, the data with 5 percent error is very accurate, but only 44 to 69 percent of the data remains after filtering (Table 3.2) which might be a problem for inversion. Therefore, injection time of 500ms is recommended with an error tolerance of 20 percent which is reasonable, for data is weighted during inversion.

Table 3.2: Valid data

	8s	1 s	500ms	250ms
Valid data % (error <20 %)	72	76	85	82
Valid data % (error <5 %)	44	51	63	69

3. Results

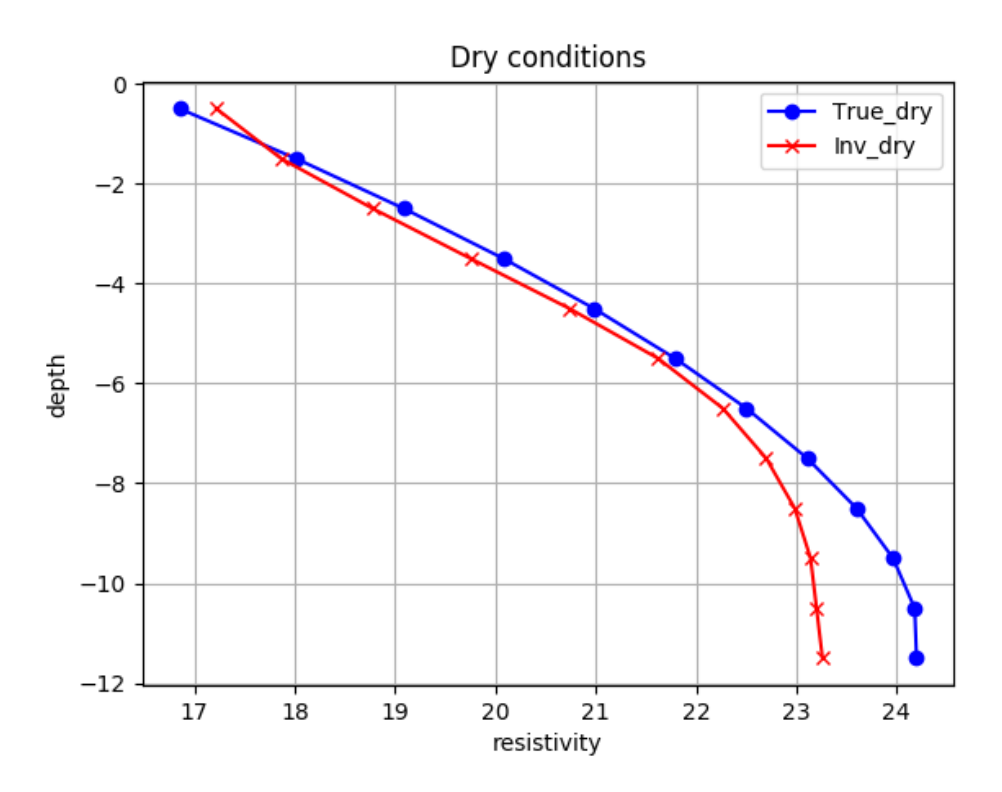


Figure 3.10: Comparison of average vertical resistivity dry scenario SF line.

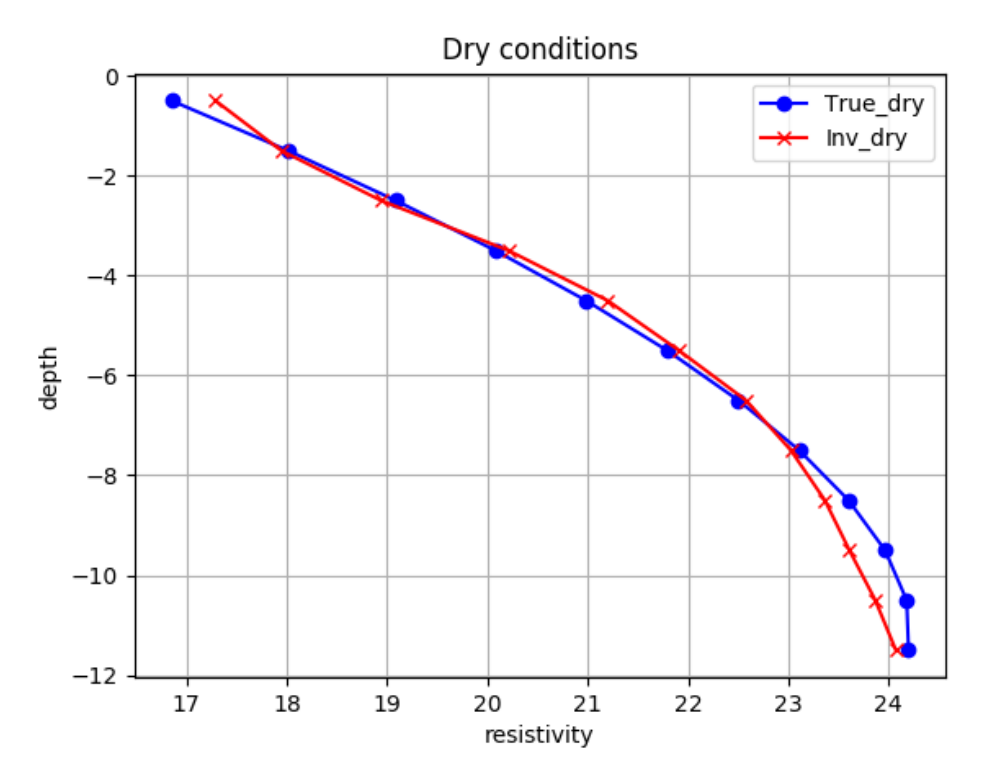


Figure 3.11: Comparison of average vertical resistivity dry scenario SF-BH line.

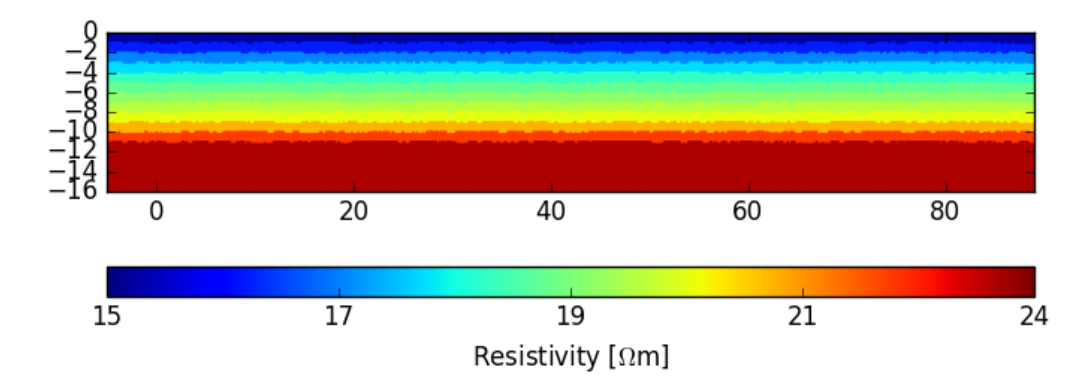


Figure 3.12: True resistivity field wet scenario.

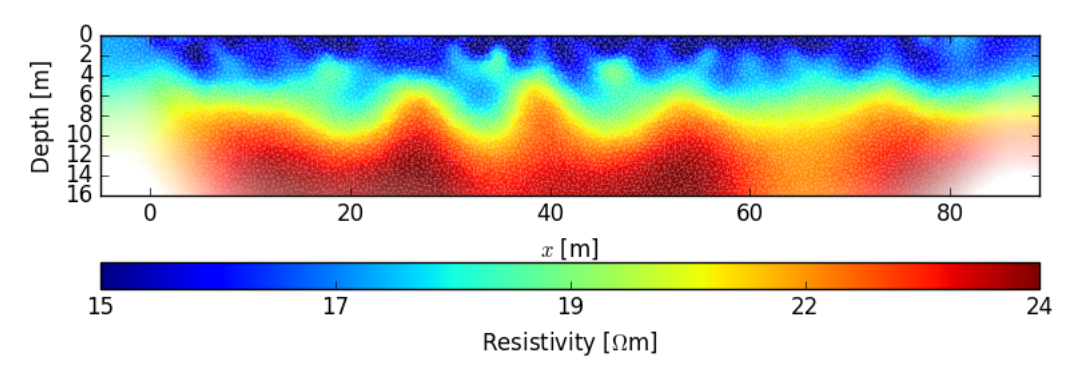


Figure 3.13: Inverted resistivity field wet scenario SF line.

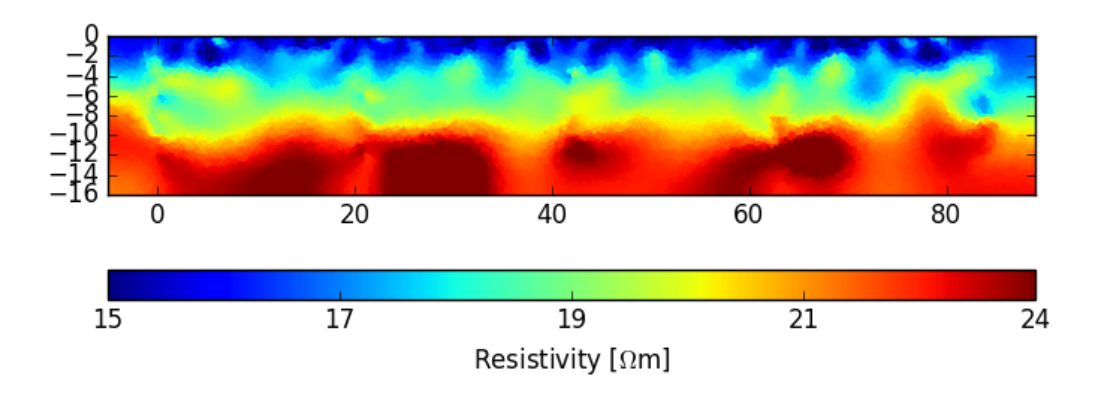


Figure 3.14: Inverted resistivity field wet scenario SF-BH line.

3. Results

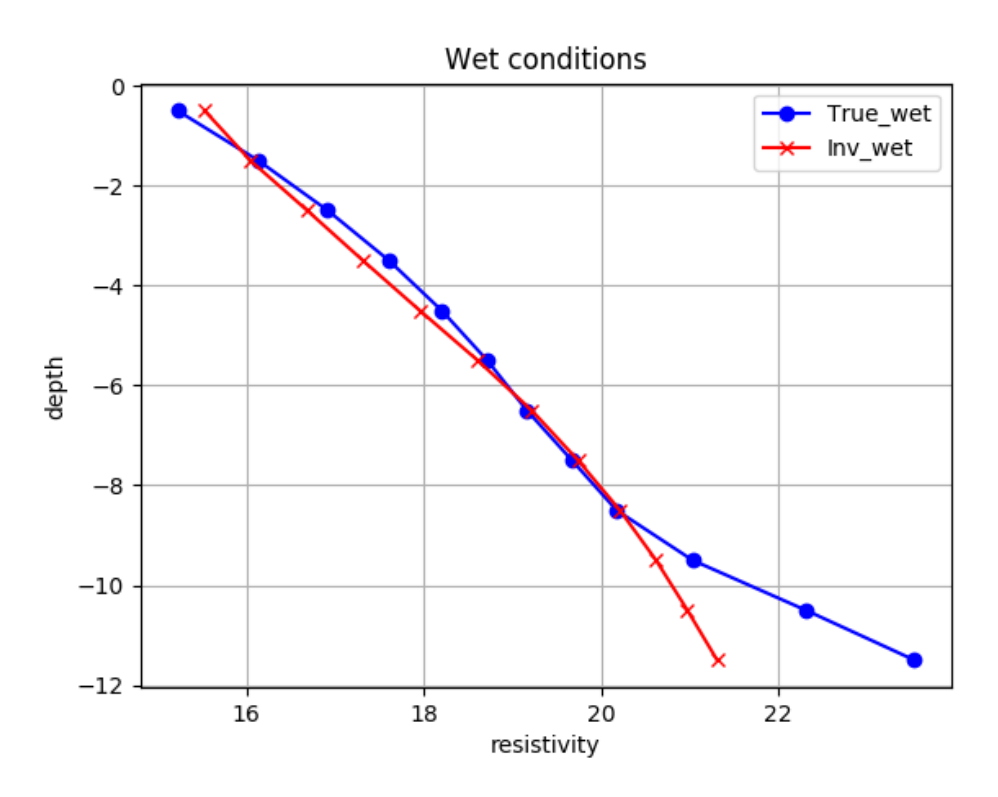


Figure 3.15: Comparison of average vertical resistivity wet scenario SF line.

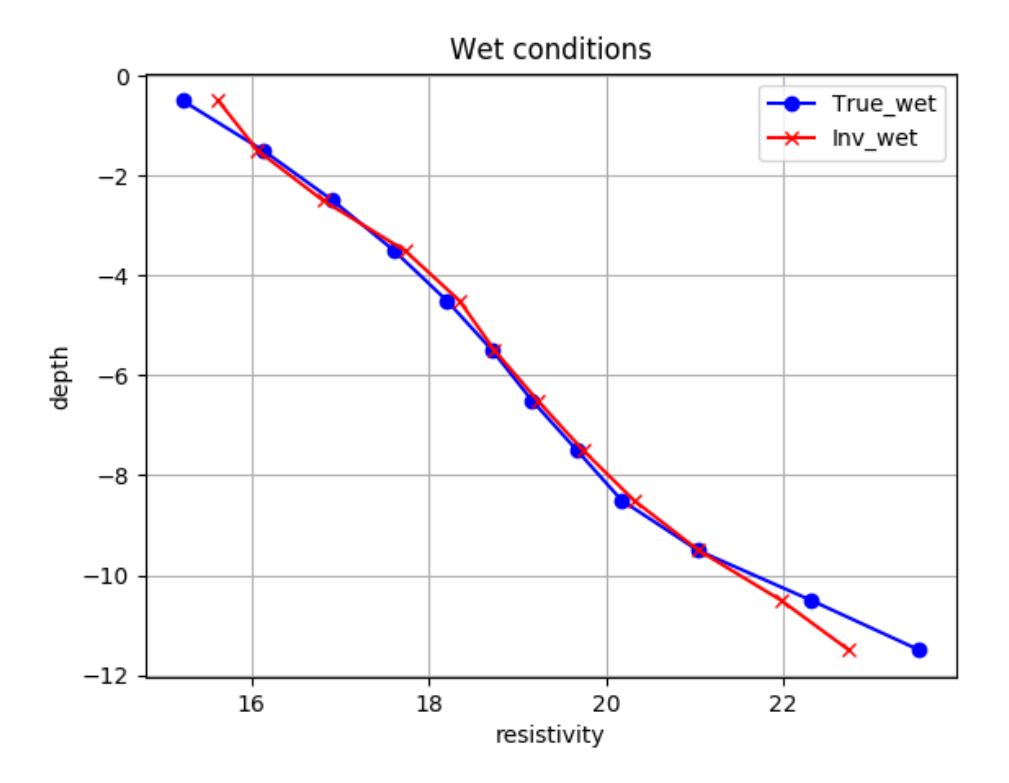


Figure 3.16: Comparison of average vertical resistivity wet scenario SF-BH line.

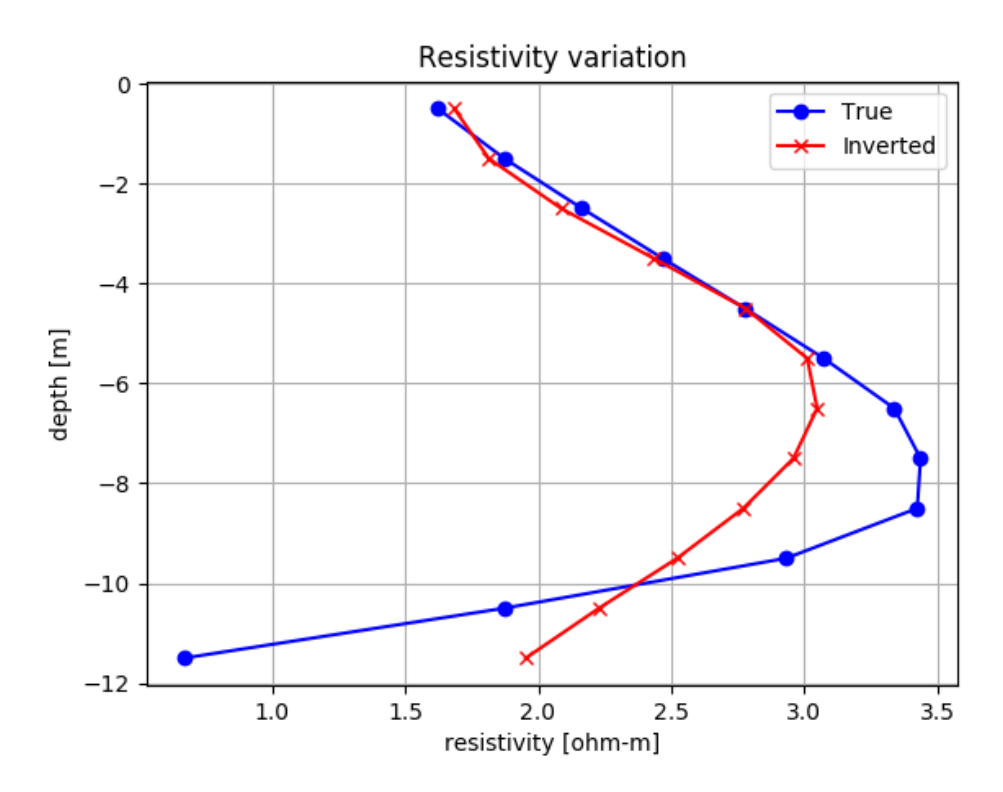


Figure 3.17: Comparison variation in vertical resistivity SF line.

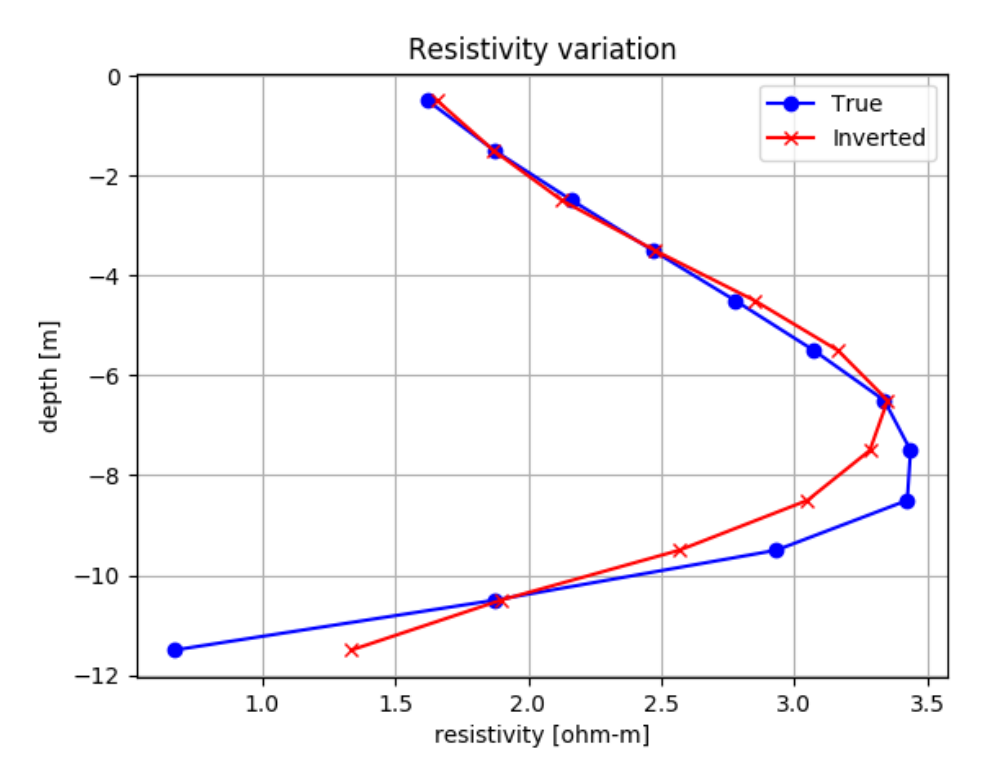


Figure 3.18: Comparison variation in vertical resistivity SF-BH line.

24 3. Results

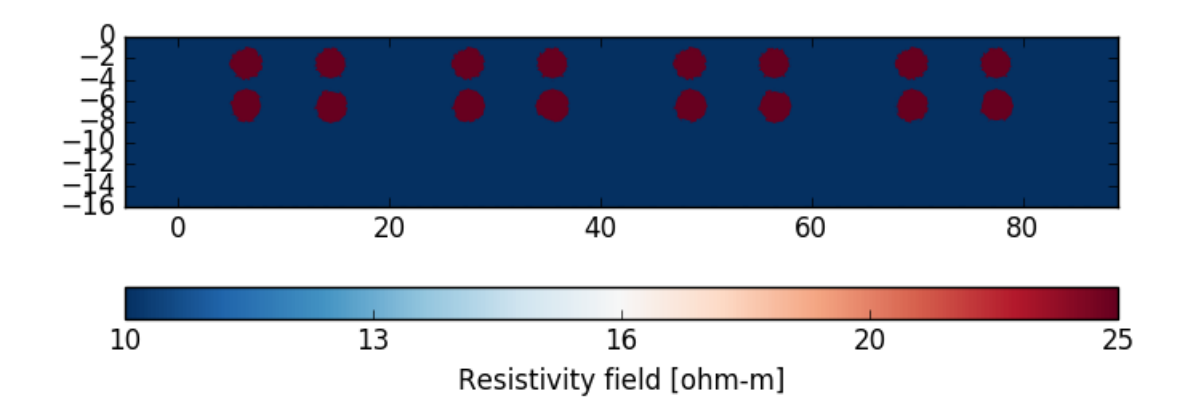


Figure 3.19: True resistivity field.

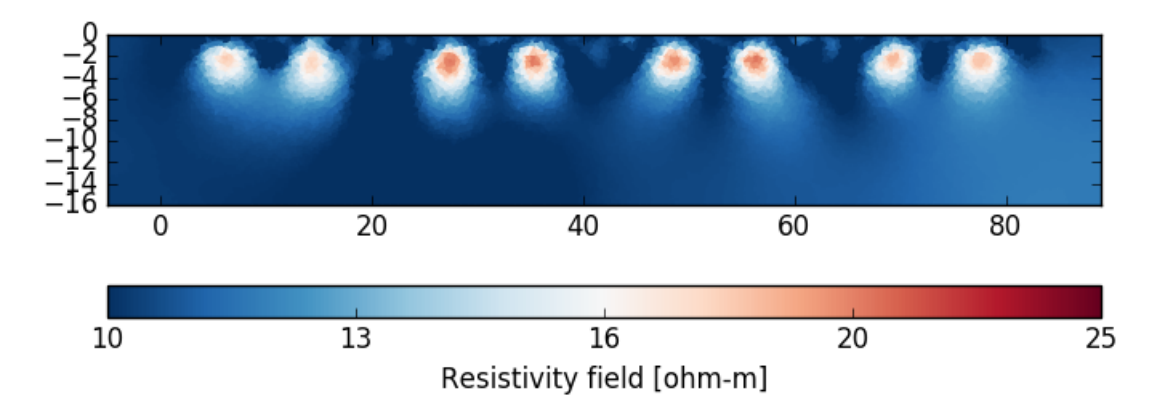


Figure 3.20: Inverted resistivity field checkerboard model SF line.

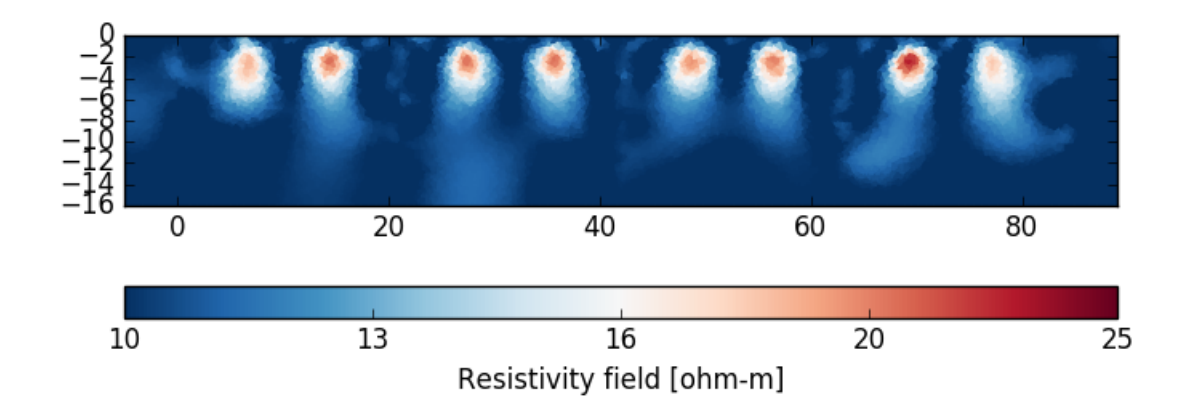


Figure 3.21: Inverted resistivity field checkerboard model SF-BH line.

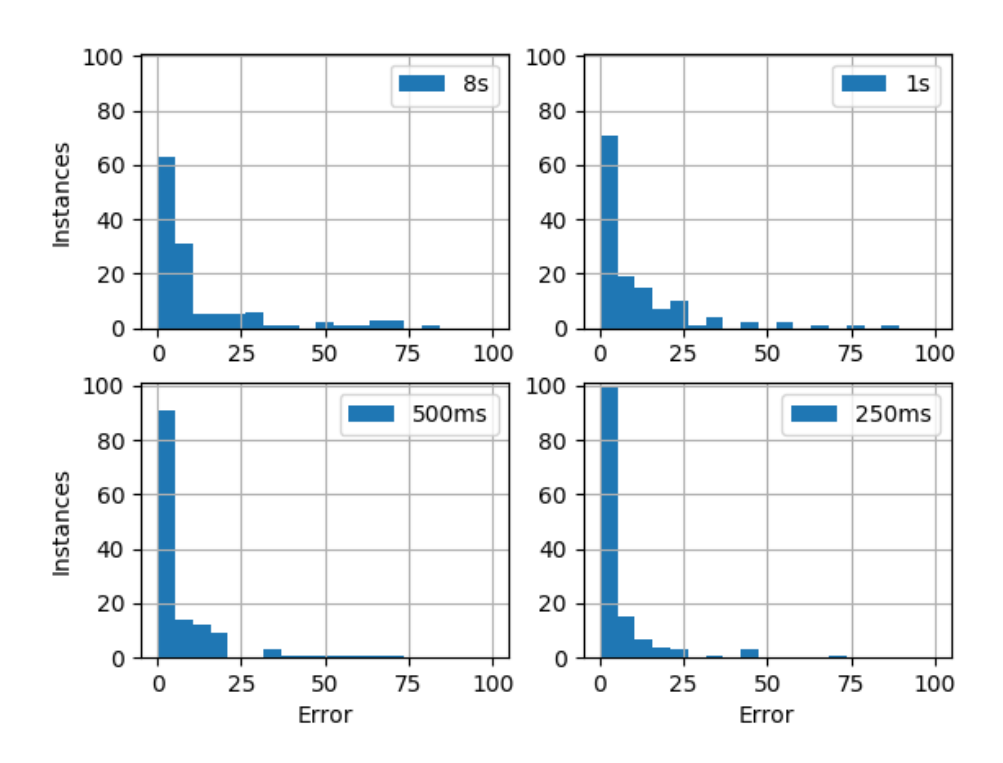


Figure 3.22: Data error histogram.

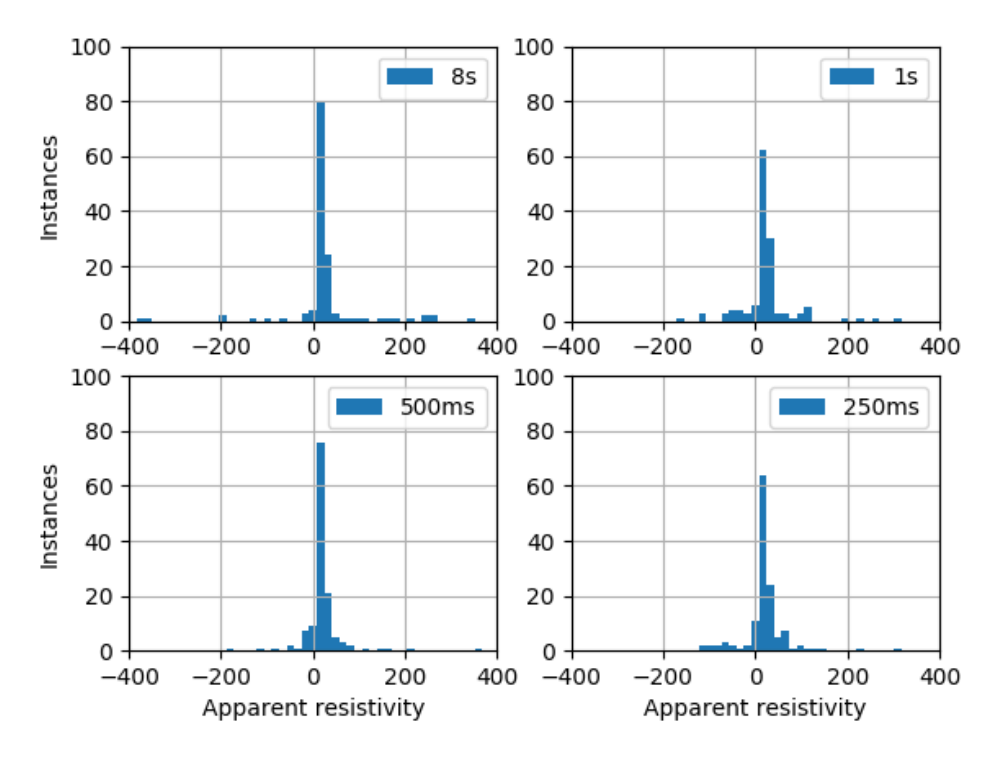


Figure 3.23: Apparent resistivity histogram.

3. Results

One to one comparison (error < 20%)

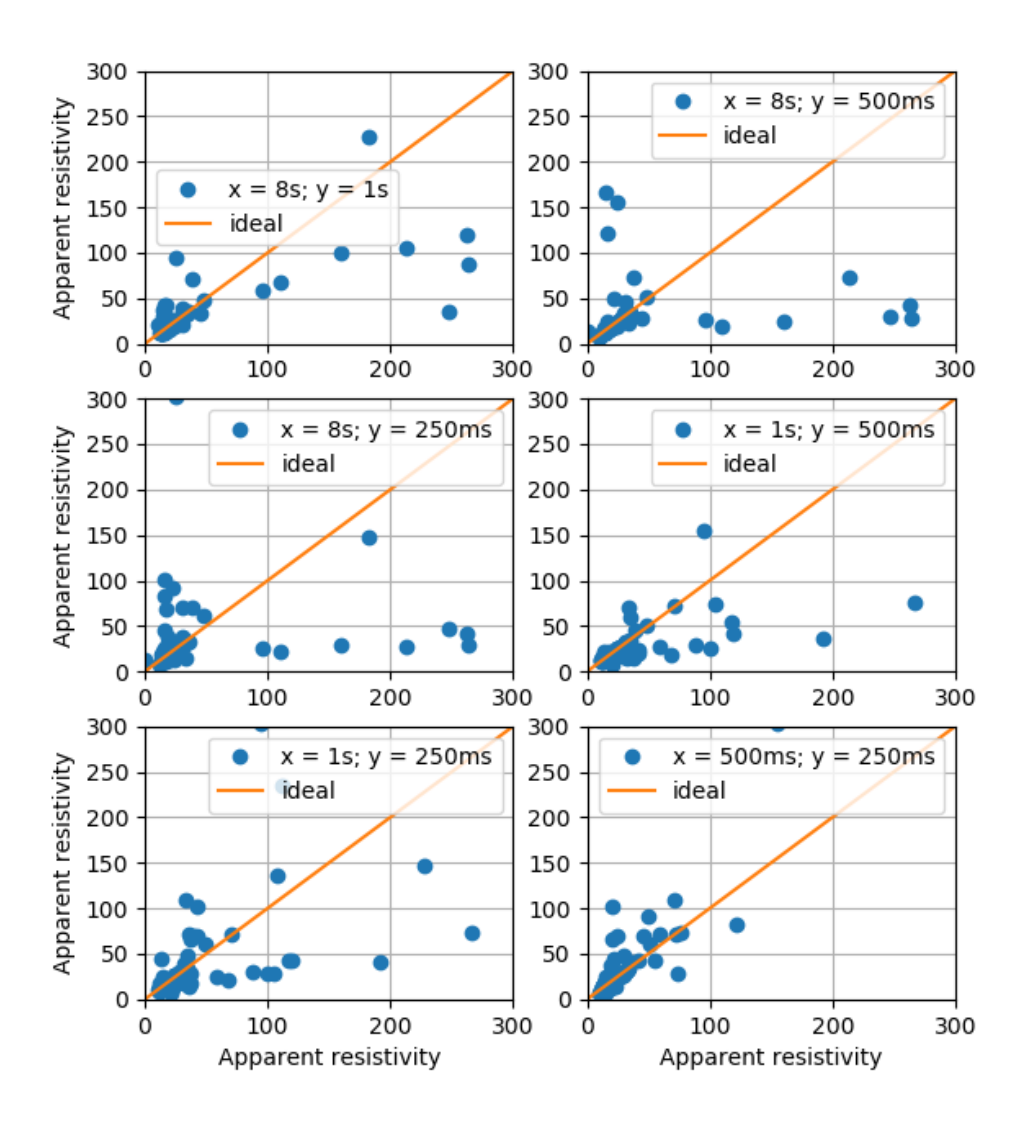


Figure 3.24: Comparison apparent resistivity (data error < 20 %).

One to one comparison (error < 5%)

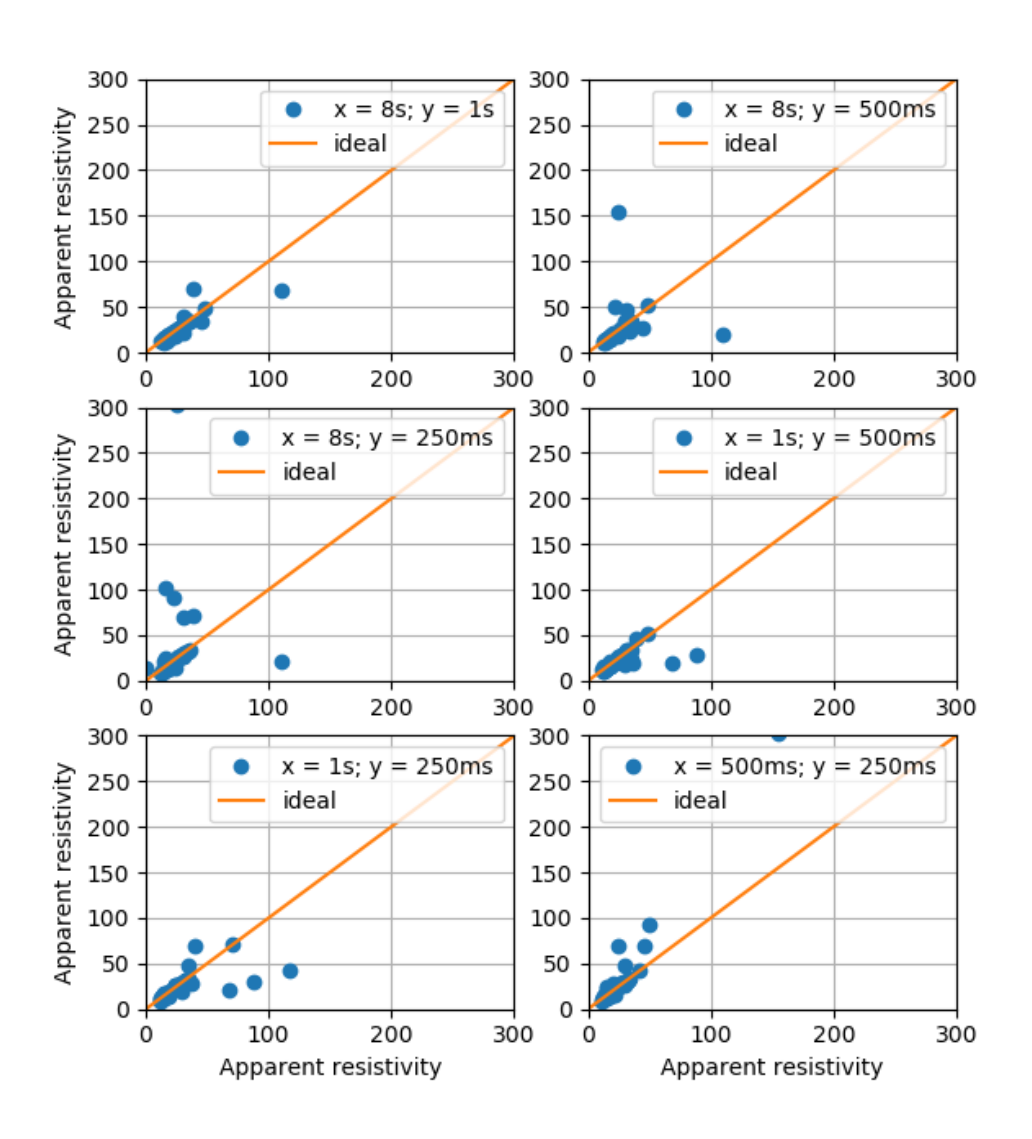


Figure 3.25: Comparison apparent resistivity (data error < 5 %).

Discussion

4.1. Part I: Spread and spacing

Building a Pareto set for finding an optimum grid is a robust approach although it is computationally expensive. Nevertheless, the Pareto set is build only once per study case, so in the end it is a feasible approach. Finding an optimum grid is crucial in order to exploit the ERT method. Otherwise, an optimum array design is not optimum when applied in a sub optimal grid. The Pareto set could also be generated for other types of exploration methods, for example, ground penetration radar.

Although two dimensional data can be used for three dimensional inversion, relevant information between lines is lost, especially if the lines are too far apart. Measurements in the transverse direction do not provide significant three-dimensional information because of the small spread of the grid in the transverse direction. The recommended approach to retrieve truly three-dimensional information is by rotating the survey direction in 90 degrees.

4.2. Part II: Array design

Applying the goodness function for array design proved to be efficient in finding the best configurations. Moreover, data acquisition in the field is fast, for the goodness function was modified for acquisition with multiple-channel systems. An alternative to the goodness function is the compare R method proposed by [11]. This method is more efficient in selecting optimal configurations, but is extremely inefficient in terms of computational time. This method could be used for further improvement of array design (selection of four-electrode configurations).

The two drawbacks found during the optimization were the size of the sensitivity matrix and the matrix inversion needed to obtain the model resolution matrix. These problems were overcome by using coarse discretization, but for larger problems this approach is not feasible anymore. Alternatively, the diagonal of the resolution matrix can be approximated with a computationally less expensive approach [19] and [20]. Parallel computation is also an alternative to increase efficiency, for example, the computation of the Hessian matrix can be parallelized. Also, the compare R method is suitable for parallelization which could be useful if combined with multiple cores in a server or in a personal computer with scientific computing capabilities in the graphical processing unit. These alternative approaches were not needed for this study, but they might be needed if the acquisition system is able to handle more electrodes or if a continuous survey extension is used.

Applying the goodness function to the SF-BH line is not recommended, for measurements that use buried electrodes might be faulty. Thus, relying on borehole measurements is not a sound approach. Instead, using a base of optimized surface measurements and use borehole information only when reliable seems to be a safer approach to guarantee data quality. The most sensitive borehole configurations should be added, so that the resolution is increased significantly in the lower part of the

30 4. Discussion

target. Instability problems during inversion are found for some borehole configurations. The root of the instability is still unknown, but it might be caused by negative values of apparent resistivity. This is an additional reason for not applying the goodness function directly to the SF-BH lines.

4.3. Part III: Array performance

For a smooth distribution of resistivities, both SF and SF-BH arrays perform well. However, for a sharp resistivity field (checkerboard), the reconstructed image is faulty for both arrays. This is a result of a sharp resistivity field inverted with smoothness regularization.

The inverted data was interpreted in terms of a one-to-one comparison between the true and inverted models which is not a robust method. Instead, statistical inversion is recommended such as that presented by Day-lewis *et al.* [21].

4.4. Part IV: Practical aspects for data acquisition

Considering practical aspects in data acquisition might improve data quality significantly. First, it is important to determine the necessary equipment settings to be used by means of a pre-design survey. Subsequently, the sequence of measurements has to be rearranged in order to reduce polarization effects. Finally, unstable configurations should be removed.

An additional practical consideration is related to the consistency of the measurements in terms of position of the electrodes, for it is crucial for comparison purposes. Although error in electrode positions is considered specifically in this study, electrodes should to be placed with high accuracy. Given the fact that these monitoring experiments are intended to last for approximately ten years, reference marks should be located in the field with a global positioning system which would also improve the operability of the survey.

5

Conclusions

Electric resistivity tomography is a promising geophysical method for monitoring waste degradation and moisture content in landfills. Consequently, an optimum survey strategy is sought in order to retrieve high resolution information while covering the largest possible area.

To achieve high resolution, the electrode spacing should be as small as possible and the spread of the electrodes as wide as possible. Nevertheless, using a dense grid of electrodes is unpractical given the need for the survey to cover a large area. On the other hand, extending the covered area, by increasing electrode spacing, reduces the resolution. Building a Pareto front with the resolution and the covered area as objective criteria proved to be an effective approach for analyzing in an objective manner different grid design alternatives. However, the final grid design choice is rather subjective, for the Pareto front is composed of several designs. The depth-average resolution was used as final criteria to choose one design from the set of designs in the Pareto front. Building a Pareto front is also a useful tool for discarding poor grid designs. This is important because some grid design alternatives might seem appealing at first sight, but when analyzed in detail, their performance is poor in the sense that they are not in the Pareto front. The optimum grid was found to have an spread of 84 meters and a spacing of 2.1 meters. This optimum grid provides good resolution in a target depth of 2.0 to 16.0 meters and is used in the subsequent step.

The set of four-electrode configurations used for data acquisition has to retrieve high resolution information. Therefore, the comprehensive set of configurations was analyzed and those configurations, standard and non standard, with the highest resolution were chosen. The configurations were analyzed with a goodness function adapted for multiple channel acquisition systems. With this criteria, 90 percent of the resolution of the comprehensive data set was achieved with only 1 percent of configurations.

Array design performance has to be tested in synthetic models before actual data acquisition. Array performance proved to be good for smooth synthetic models, for the model is in accordance with the regularization used for data inversion. On the other hand, sharp synthetic models are not well reproduced after data inversion which is a limitation of the geophysical method and not of the design. Buried electrodes improved significantly the information retrieved in the deeper parts of the target.

Data collected in the monitoring program is to be compared qualitatively and quantitatively during the coming years. Therefore, data quality is an crucial factor to consider. Pre-design surveys were carried out in order to define properly the hardware settings. Moreover, error has to be minimized by removing geometrically sensitive configurations and by rearranging the injection sequence, so that polarization effects are reduced. These type of considerations are often overlooked which produces poor data quality. An injection time of 500 ms showed less outliers data compared to 8000, 1000 and 500 ms and was chosen for field survey.

In brief, this thesis presents a protocol for monitoring landfills with electrical resistivity tomography aiming to acquire high resolution data, but at the same time being practical for monitoring the exper-

32 5. Conclusions

iments in the years to come. Although this protocol consider major issues for the generation of an optimum survey strategy, it does not cover all. In that sense the protocol is intended as a basic guideline, so it leaves room for improvement and inclusion of additional features depending on the specific application which is not limited to landfill monitoring nor to electric resistivity tomography. Finally, the acquired data is significant only if it gives insight into the system that is being analyzed, so the data should be joined to other type of model such as a hydrogeological model.

Bibliography

- [1] W. van Vossen and K. Heyer, Feasibility study sustainable emission reduction at the existing landfills Kragge and Wieringermeer in the Netherlands. Preliminary design and cost-estimate of the technical measures infiltration and aeration to enhance stabilization at the landfill Wieri, , 51 (2009).
- [2] A. van Turnhout and T. J. Heimovaara, *Optimal coupled model of water flow, mass transport and biogeochemical activity to predict emission behavior of landfills,* , 1 (2016).
- [3] S. Baviskar, *The origin of preferential flow and non-equilibrium transport in unsaturated heterogeneous porous systems,* (2016), 10.4233/uuid:faedef77-b7dc-47c7-a6d5-891e95baab70.
- [4] S.-A. Korteland, Quantitative Characterization of Solute Transport Processes in the Laboratory Using Electrical Resistivity Tomography (2013).
- [5] P. Y. Papalambros and D. J. Wilde, *Principles of Optimal Design* (Cambridge University Press, 2000) p. 390.
- [6] W. Menke, *Chapter 1 Describing Inverse Problems*, Geophysical Data Analysis: Discrete Inverse Theory (Third Edition) , 1 (2012).
- [7] T. Günther, C. Rücker, and K. Spitzer, *Three-dimensional modelling and inversion of dc resistivity data incorporating topography II. Inversion*, Geophysical Journal International **166**, 506 (2006).
- [8] M. H. Loke, P. B. Wilkinson, S. S. Uhlemann, J. E. Chambers, and L. S. Oxby, Computation of optimized arrays for 3-D electrical imaging surveys, Geophysical Journal International 199, 1751 (2014).
- [9] Z. Bing and S. Greenhalgh, A synthetic study on crosshole resistivity imaging using different electrode arrays, Exploration Geophysics 28, 1 (1997).
- [10] M. Noel and B. Xu, *Archaeological investigation by electrical resistivity tomography: a preliminary study,* Geophysical Journal International **107**, 95 (1991).
- [11] P. B. Wilkinson, P. I. Meldrum, J. E. Chambers, O. Kuras, and R. D. Ogilvy, *Improved strategies* for the automatic selection of optimized sets of electrical resistivity tomography measurement configurations, Geophysical Journal International **167**, 1119 (2006).
- [12] P. Stummer, H. Maurer, and A. G. Green, Experimental design: Electrical resistivity data sets that provide optimum subsurface information, GEOPHYSICS 69, 120 (2004).
- [13] A. van Turnhout, H. Oonk, H. Scharff, and T. J. Heimovaara, *Optimizing landfill aeration strategy with a 3-D multiphase model,* **20**, 1.
- [14] S. Grellier, K. R. Reddy, J. Gangathulasi, R. Adib, and C. C. Peters, *Correlation Between Electrical Resistivity and Moisture Content of Municipal Solid Waste in Bioreactor Landfill*, in *Geoenvironmental Engineering*, 163 (American Society of Civil Engineers, Reston, VA, 2007) pp. 1–14.
- [15] F. D. Day-Lewis, C. D. Johnson, K. Singha, and J. W. J. Lane, *Best practices in electrical resistivity imaging: Data collection and processing, and application to data from Corinna, Maine,* (2008).
- [16] P. B. Wilkinson, M. H. Loke, P. I. Meldrum, J. E. Chambers, O. Kuras, D. A. Gunn, and R. D. Ogilvy, *Practical aspects of applied optimized survey design for electrical resistivity tomography,* Geophysical Journal International **189**, 428 (2012).

34 Bibliography

[17] P. B. Wilkinson, J. E. Chambers, M. Lelliott, G. P. Wealthall, and R. D. Ogilvy, *Extreme sensitivity of crosshole electrical resistivity tomography measurements to geometric errors*, Geophysical Journal International **173**, 49 (2008).

- [18] F. M. Wagner, T. Günther, C. Schmidt-Hattenberger, and H. Maurer, *Constructive optimization of electrode locations for target-focused resistivity monitoring*, GEOPHYSICS **80**, E29 (2015).
- [19] C. Bekas, E. Kokiopoulou, Y. Saad, C. Science, and T. Cities, *An Estimator for the Diagonal of a Matrix* \square , , 1 (2005).
- [20] J. K. Maccarthy, B. Borchers, and R. C. Aster, *Efficient stochastic estimation of the model resolution matrix diagonal and generalized cross–validation for large geophysical inverse problems*, **116**, 1 (2011).
- [21] F. D. Day-lewis, K. Singha, and A. M. Binley, *Applying petrophysical models to radar travel time and electrical resistivity tomograms: Resolution-dependent limitations,* **110**, 1 (2005).